JOURNAL OF FUEL CHEMISTRY AND TECHNOLOGY
Volume 54, Issue 8, August 2026

燃料化学学报(中英文)
Journal of Fuel Chemistry and Technology

Cite this article as: J Fuel Chem Technol, 2026, 54, 20250321

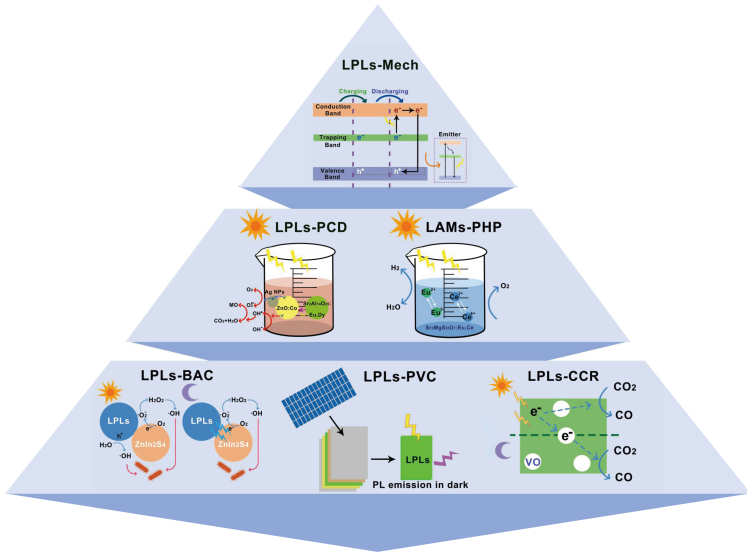
REVIEW

Clean and green: Harnessing long persistent luminescence for advanced catalysis

HUANG Haiyan[1], YANG Yarong[1], ZHAO Zhuoya[1], LIU Dingyi[1], WANG Xuan[1], WU Shuqi[1,*], QIN Yong[2,*], MIAO Jiaojiao[1,*]

[1] Interdisciplinary Research Center of Biology & Catalysis, School of Life Sciences, Northwestern Polytechnical University, Xi'an 710072, China;
[2] College of Material Science and Engineering, Qingdao University of Science and Technology, Qingdao 266042, China

Abstract: Long persistent luminescence materials (LPLMs) have demonstrated significant potential in the field of photo- and electro-catalysis due to their unique capability of storing and controllably releasing photogenerated charge carriers. These materials offer innovative solutions for environmental remediation and sustainable energy technologies. This review systematically summarizes recent advances in the application of LPLs in photo- and electro-catalysis, outlining their developmental history and underlying mechanisms. Emphasis is placed on their applications in organic pollutant degradation, photocatalytic hydrogen evolution, and photovoltaic cells. Furthermore, design strategies and research frameworks for LPLs are discussed. The current limitations and challenges in this field are examined, and future research directions are proposed to facilitate the transition of LPLMs from fundamental research to practical applications in energy and the environment.



Key words: catalysis; long persistent luminescence (LPL); degradation; hydrogen; solar energy

Luminescent materials are non-thermal radiation functional materials that undergo energy conversion through excitation by light, electricity, or chemical energy. Long persistent luminescent materials (LPLMs) are a special category of photoluminescent materials. The unique trap levels enable the storage of excited-state charge carriers and delayed release, allowing LPLMs to continue emitting light for minutes to several days after the excitation ceases, with emission wavelengths covering the ultraviolet to near-infrared (UV-NIR) range[1–4]. Initial research on long-persistent luminescent materials primarily focused on covert illumination and safety signage applications. The surge in military air defense demands during World War II significantly accelerated the technological evolution and large-scale production of this system. Sulfide-based materials (e.g., ZnS:Cu) represent the first commercially viable long-persistent luminescent system, offering advantages such as broad emission spectra and rapid response to low-light excitation. However, these materials suffer from issues including low persistent brightness, short persistence duration, and susceptibility to moisture and oxidation. Although later improvements were attempted—such as incorporating radioactive isotopes (e.g., ^{147}Pm and tritium ^{3}H) as internal excitation sources or applying protective surface coatings—these materials ultimately remained limited in application due to inherent

Received: 2025-10-29; Revised: 2025-12-22
* Corresponding author. E-mail: sqwu@nwpu.edu.cn, qinyong@qust.edu.cn, mjj.smile@nwpu.edu.cn.
DOI: 10.1016/S1872-5813(26)60692-5 CSTR: 32157.14.2097-213X.2026.JFCT.0050
本文的英文电子版由 Elsevier 出版社在 ScienceDirect 上出版 (http://www.sciencedirect.com/science/journal/18725813)

safety concerns and stability issues[5−8]. Around 1960, Japanese researchers first observed long afterglow in $SrAl_2O_4$:Eu^+[9]. In 1996, Matsuzawa et al.[10] incorporated trivalent rare-earth elements into this system to optimize trap distribution, developing $SrAl_2O_4$:Eu^+, Dy^+ long-afterglow materials. The afterglow originates from the $5d \rightarrow 4f$ transition of Eu^+, enabling green afterglow (520 nm) lasting up to 30 h. This breakthrough marked a major milestone in the field of LPLMs and rapidly spurred the commercialization of aluminate-based long-afterglow materials. Thanks to their improved safety and chemical stability, these green LPLs are now widely used in public safety and consumer products, including emergency signage, luminous pavement or runway markings, ceramic printing, and luminous watch dials[11]. In addition, LPLs show great potential in the fields of biomedical science, archival storage, clean energy and environmental protection due to their unique energy storage and controllable release characteristics (Figure 1).

In the biomedical field (Figure 1), long persistent luminescent materials (LPLMs) have been extensively applied in autofluorescence-free biosensing, long-term real-time deep-tissue imaging, theranostics, and X-ray imaging[12]. As an ideal alternative to traditional fluorescent probes, LPLMs enable temporal separation between excitation and emission. This eliminates the need for *in situ* excitation, thereby avoiding background interference from tissue autofluorescence and scattered light. Simultaneously, their excellent near-infrared afterglow properties, high responsivity, and excellent tissue penetration collectively enhance the signal-to-noise ratio and detection sensitivity[13]. Shallow-trap LPLMs readily undergo de-trapping at room temperature and have been widely applied in security labeling and in vivo bioimaging. However, photons stored in deep-trap LPLMs are not easily released under ambient conditions. This characteristic makes them promising for data storage (Figure 1), where the trapping and controlled de-trapping processes at room temperature can serve as a means for data writing and reading, enabling high-capacity optical storage. By leveraging the distinct emission spectra associated with different deep trap levels, multi-level data storage can be achieved through spectral multiplexing of the released photons[14].

The deterioration of the natural environment and the ongoing energy crisis are two major challenges facing modern society. In recent years, long persistent luminescent materials (LPLMs) have also demonstrated unique advantages in the fields of clean energy and environmental protection due to their photo-/electrocatalytic properties. Photo-/electrocatalysis harnesses solar energy to drive CO_2 conversion, water splitting, and pollutant degradation, offering a promising pathway toward energy transition and environmental remediation. However, conventional photocatalytic materials often suffer from limitations such as rapid carrier recombination and low light utilization efficiency[15−18]. LPLMs achieve controllable release of excited-state energy (ranging from seconds to hours) by constructing an energy level structure that synergize deep and shallow traps. This capability offers a promising pathway to address the following core challenges: (1) achieving broad-spectrum absorption to enhance light utilization; (2) enabling the slow release of trapped electrons to prolong carrier lifetime and improve catalytic efficiency. Research on LPLMs in the fields of photocatalysis and electrocatalysis continues to grow, demonstrating their considerable potential in addressing energy and environmental issues. However, comprehensive reviews in this area remain relatively scarce. Therefore, this paper aims to systematically review the research progress of LPLMs in photo-/electrocatalysis, with a focus on their application cases and material design strategies, including pollutant degradation, photocatalytic hydrogen evolution, photovoltaic cells, CO_2 reduction, and photocatalytic antimicrobial disinfection (Figure 2).

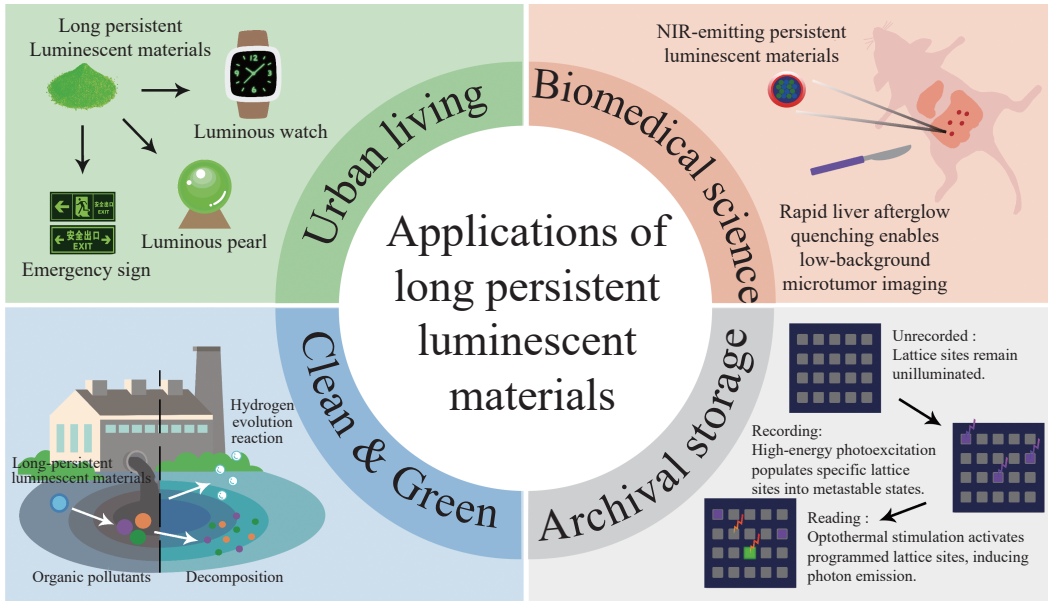


Fig. 1 Schematic of LPLMs applications across urban living, biomedical science, archival storage, and clean and green

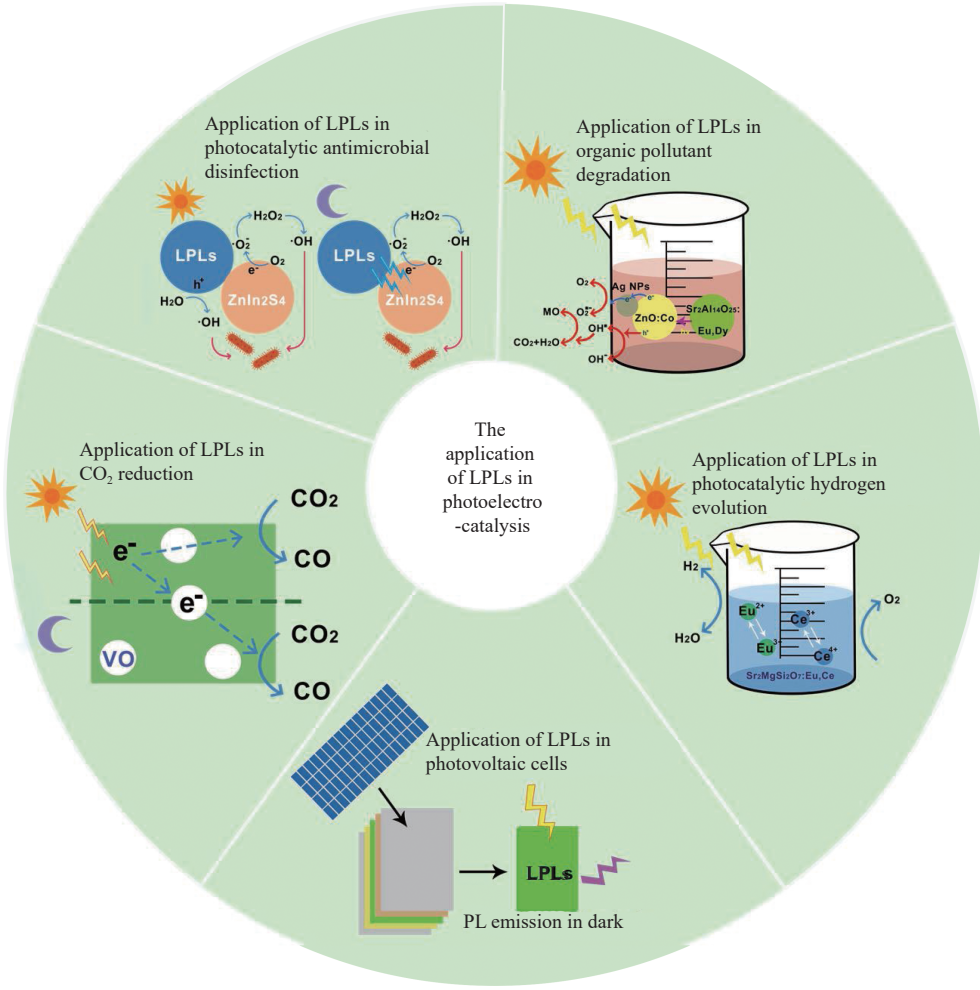


Fig. 2 Schematic diagram of the applications of LPLMs in photo-/electrocatalysis, including organic pollutant degradation, photocatalytic hydrogen evolution, photovoltaic cells, CO_2 reduction, and photocatalytic antimicrobial disinfection

Furthermore, it analyzes current performance bottlenecks and outlines future research directions. The aim is to promote the innovative application of long-afterglow materials in clean energy technologies through an interdisciplinary perspective, accelerating their transition from fundamental research to engineering and practical implementation.

1 Long afterglow materials: mechanisms in photo- and electrocatalysis

The mechanism of long persistent luminescent materials (LPLMs) can be summarized in the following steps[19–21] (Figure 3). First, LPLMs are excited by external energy sources—such as ultraviolet light, visible light, high-energy rays, or electron beams—generating delocalized and mobile charge carriers (electrons or holes). Second, excited carriers can be captured by electron/hole traps through migration in the conduction or valence bands, or *via* quantum tunneling between energy levels within the forbidden gap. This capture process allows the traps to store excitation energy for extended periods, after which the trapped carriers are gradually released from the traps. The depth of the trap and external fields such as thermal, optical, or mechanical perturbations can influence the release rate of charge carriers stored within the traps. Finally, carrier recombination occurs, where released carriers migrate back to the emission centers, resulting in delayed luminescence due to electron-hole recombination produces (Figure 3). The advantage of long persistent luminescence materials lies in the metastable trap levels within the bandgap. The charge carriers are stored in trap levels, effectively inhibiting their immediate recombination during the fluorescence process.

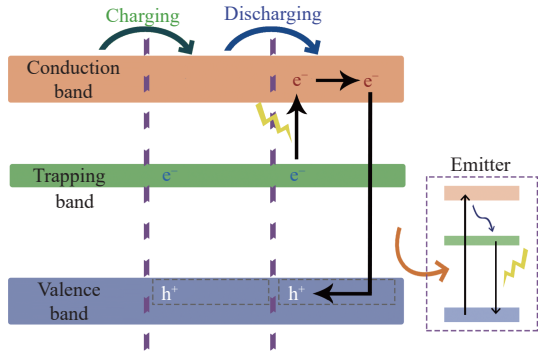


Fig. 3 Schematic diagram of electron transfer and phase diagram for LPLs in long-lasting phosphorescent materials

Materials with long afterglow for properties employed in photo-/electrocatalysis are predominantly inorganic systems[19], so this paper focuses on the mechanism of inorganic LPLMs. Organic long-afterglow systems, whose mechanism is largely based on molecular excited-state energy release or chemical reactions[22], are not discussed here.

Inorganic long persistent luminescent materials (LPLs) typically consist of a host lattice, activators, and co-activators, and generally feature two types of active centers: an emission center and a trap center. Emission centers are mainly classified into three categories: (1) lanthanide ions (e.g., Ce^{3+}, Eu^{2+}, Nd^{3+}, Er^{3+}) exhibiting $5d\rightarrow4f$ or $4f\rightarrow4f$ transitions; (2) transition-metal ions (e.g., Cr^{3+}, Mn^{2+}, Mn^{4+}, Ni^{2+}) showing $d\rightarrow d$ transitions; (3) main-group or post-transition metal ions (e.g., Pb^{2+}, Bi^{3+}) involved in $p\rightarrow s$ transitions. The emission center primarily determines the spectral region of the emitted light, while the properties of the trap center govern the afterglow intensity and duration at a given temperature. Traps can form through three mechanisms: lattice/intrinsic defects (e.g., oxygen vacancies, F color centers, cation antisite defects), impurity ions (e.g., Ti^{3+}, Cu^{2+}), or lanthanide/d-metal ions as dopants or co-dopants. Co-doping serves as one effective strategy for capturing charge carriers, enabling metastable trap levels to approach the conduction or valence band of the host lattice. Charge transfer between dopant and co-dopant can further prolong luminescence; under certain conditions, the emission center itself may also act as a trap center[19,21]. Trap characteristics of traps typically involve three aspects: defect type, effective trap concentration, and effective trap depth[4,18,23−28]. (1) Investigating trap types focuses on identifying the corresponding defect categories and verifying whether these defects effectively involvement in carrier capture process. Generally, traps originate primarily from various lattice defects within the material. For instance, compounds grown under high temperature and pressure develop dislocations due to thermal stress, or a creep process, rendering these defects as effective carrier traps. However, accurately identifying the specific trap type is challenging, and determining which defect dominates the capture process is even more difficult; (2) Effective trap concentration represents the number of active traps capable of capturing charge carriers. Increasing the effective trap concentration allows more electrons to be captured, thereby enhancing the material's electron storage capacity—a key factor in prolonging afterglow lifetime (or sustained catalytic duration); (3) The effective trap depth determines the release rate of trapped charge carriers and fundamentally influences the intensity and duration of the afterglow. In an energy band diagram, trap depth corresponds to the activation energy required for an electron to transition from the trap level to the conduction band (or for a hole to transition to the valence band). Extremely shallow traps undergo simultaneous trapping and de-trapping at room temperature, making afterglow difficult to observe. Shallow traps exhibit high release rates at room temperature, leading to rapid depletion of trapped carriers, which facilitates the attainment of strong initial afterglow intensity. Deep traps release carriers slowly and show almost no depletion at room temperature, resulting in weak afterglow intensity but extended duration. The deeper the trap, the higher the activation energy required; therefore, afterglow from very deep traps is typically not observable under ambient conditions. It is generally accepted that trap depths close to the conduction or valence band edge (approximately 0.6−1 eV) provide optimal conditions for observing pronounced afterglow at room temperature.

Understanding the underlying mechanism is a crucial aspect of long persistent luminescent materials (LPLs). While the fundamental principles of persistent luminescence have become increasingly clear, the precise mechanisms governing the capture and release of charge carriers are still a controversial issue. Currently, the three most widely accepted models (Figure 4) are the conduction band-valence band (CB-VB) model, the hole transport model, and the quantum tunneling (QT) model[29−30]. The CB-VB model (Figure 4) indicates that most excited electrons form fluorescence by relaxing non-radiatively to the lowest energy level and return to the ground state. A minority of electrons are captured by defect energy levels (traps) during relaxation, elevating the ion valence state. When trapped electrons acquire sufficient thermal energy from the environment, they can escape to an excited state. Their eventual return to the ground state, accompanied by a reduction in valence and the release of a photon, results in long afterglow emission. The hole transport model (Figure 4) demonstrates that under visible or ultraviolet light excitation, the excited-state electrons generated in the material can be captured by specific ions to undergo reduction. Correspondingly, the generated holes can migrate within the valence band and oxidize other ions (increasing their oxidation state). After external excitation ceases, trapped holes can escape the trap and return to the valence band by gaining sufficient energy from thermal energy (thermal escape) or interionic resonant energy transfer mechanisms. Simultaneously, the previously reduced ions recombine with these returning holes, releasing photons and generating long afterglow luminescence. Among these, shallowly trapped electrons can return to the ground state through thermal escape, whereas deeply trapped electrons are difficult to release *via* this mechanism. To account for the phenomenon of ultra-long afterglow lasting tens of hours or longer, researchers proposed the quantum tunneling model (Figure 4). Long persistent luminescent materials (LPLs) serve a dual function as both luminophores and electron-storage media. During illumination, they can act as reservoirs for photoexcited carriers, overcoming the surface-limited nature of conventional photocatalytic reduction reactions. Under dark conditions, the electrons and holes stored in LPLs during the irradiation can be transferred to an electrolyte and directly participate in catalytic reactions[28].

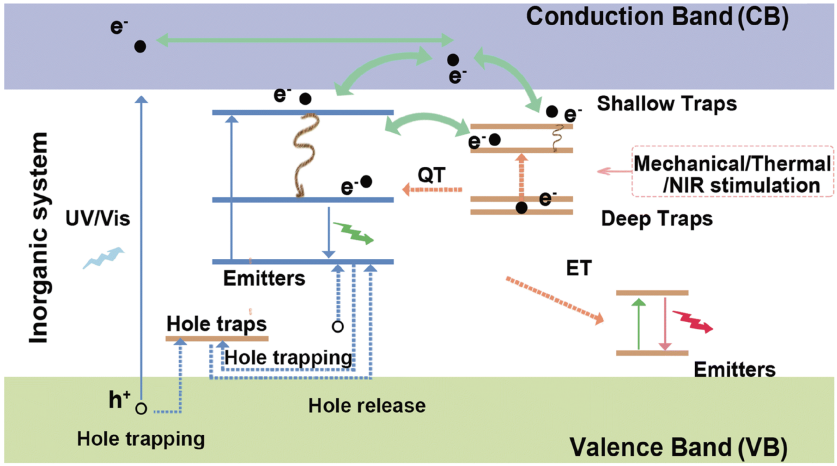


Fig. 4 Schematic diagrams of the luminescence mechanisms in LPLs (conduction band (CB)-valence band (VB) model, hole transport model, and quantum tunneling (QT) model)[27]
(with permission from Springer Nature)

This characteristic ingeniously overcomes the reliance of traditional photocatalytic reactions on continuous light sources. Consequently, LPLs are promising for photo-/electrocatalytic applications, especially in solar-driven processes such as pollutant degradation, water splitting for hydrogen production, and solar cells. Specific applications and detailed mechanisms of LPLs in photo-/electrocatalysis will be further elaborated in the case studies presented in subsequent sections.

2 Long persistent luminescent materials enable continuous photocatalytic degradation of organic pollutants

Air and water pollution by organic compounds has emerged as a major global environmental challenge in the 21st century[31]. Typical organic pollutants, such as volatile acetaldehyde, methylene blue (MB) and crystal violet (CV), can pose a threat to human health through air diffusion or bioaccumulation in the food chain, leading to respiratory diseases, allergic reactions, and even neurological damage[32−34]. Conventional treatment methods, including adsorption, membrane filtration, and chemical precipitation etc., are widely used but suffer from high cost, low degradation efficiency, and potential secondary pollution issues. Biological approaches are easily inhibited by high pollutant concentrations and exhibit limited effectiveness against refractory organic compounds[35]. Therefore, green, efficient photocatalytic technology that produces no secondary pollution has garnered widespread attention. This technology generates electron-hole pairs through light excitation of the catalyst, thereby driving redox reactions to achieve complete degradation of pollutants[36]. However, traditional photocatalysts commonly suffer from critical bottlenecks such as deactivation under dark conditions and narrow spectral response ranges, which limit their practical application efficiency[37]. Long persistent luminescent materials (LPLs) offer a promising route to overcome these limitations by virtue of their unique "store-and-release" capability of light energy[38]. Recent studies have demonstrated the significant potential of LPLs in the photocatalytic degradation of organic compounds, providing new perspectives for environmental remediation and energy conversion. Based on their composition and mechanism of action, these materials can generally be classified into two categories: one is composite long-afterglow catalysts (composite systems), which are constructed by combining LPLs with traditional catalysts; the other is single-phase long-afterglow catalysts (single-phase systems), in which the LPL itself exhibits dual functionality of both catalysis and energy storage (Tables 1 and 2).

2.1 Composite long persistent luminescent materials for continuous photocatalytic degradation of organic pollutants

In 2004, Zhang et al. constructed a multi-layer composite long afterglow catalyst by coating $Sr_4Al_{14}O_{25}:Eu^{2+},Nd^{3+}$ on the surface of TiO_2 catalyst, achieving the first-ever photodegradation of Rhodamine B under dark conditions. This study marks the formal commencement of applied research on long afterglow materials in the field of photo-/electrocatalysis. This work not only pioneered a new paradigm of "light storage-sustained release catalysis", but also laid the foundation for applying long afterglow-semiconductor composite catalysts in pollutant degradation[39]. In order to systematically sort out the development of this field, the following will be classified according to the general matrix types of long afterglow materials, and related research will be introduced in chronological order to help readers grasp the research history and current status of such catalysts in the field of photocatalysis /electrocatalysis.

Table 1 Composite long persistent luminescent catalysts for photocatalytic organic degradation

LPLs	Catalysts	Emission peak	Target pollutants	Degradation efficiency	Reference
$CaAl_2O_4:Eu^{2+},Nd^{3+}$	$TiO_{2-x}N_y$	440 nm	acetaldehyde	100%/2 h (light)	[21]
	Pt/Ag_3PO_4	440 nm	Rhodamine B	81.7%/5 h (dark)	[42]
$Sr_4Al_{14}O_{25}:Eu^{2+},Dy^{3+}$	ZnO:Co /Ag	495 nm	methyl orange	77.9%/3.5 h (dark)	[43]
$SrAl_2O_4:Eu^{2+},Dy^{3+}$	$g\text{-}C_3N_4$	520−550	basic fuchsin	90%/3 h (dark)	[46]
	$g\text{-}C_3N_4/Bi_2WO_6/WO_3$	420−580 nm	basic blue	98%/1 h (light) 87%/0.33 h (low light)	[45]
	$g\text{-}C_3N_4@NH_2\text{-}UiO\text{-}66$	520 nm	methyl blue	50%/5 h (dark)	[47]
	Cu_2O/TiO_2	430−520 nm	Rhodamine B	98%/24 h (light+dark)	[44]
			Bisphenol	93%/24 h (light+dark)	
$Sr_2MgSi_2O_7:Eu^{2+},Dy^{3+}$	Ag_3PO_4	470 nm	methyl orange	32%/0.33 h (dark)	[49]
	$g\text{-}C_3N_4$	468 nm	methylene blue	50%/5 h (dark)	[48]
	$ZnIn_2S_4/UiO\text{-}66\text{-}NH_2$	470 nm	Rhodamine B	86.7%/4 h (dark)	[50]
			methylene blue	96.8%/6 h (dark)	
$Sr_{2.90}Eu_{0.03}Dy_{0.07}Al_4SiO_{11}$	$N\text{-}TiO_2$	440 nm	crystal violet	90%/1 h (light+dark)	[51]
$Zn_3Ga_2Ge_2O_{10}$:0.5% Mn	NH_2-MIL-101(Fe)	535 nm	Rhodamine B	98%/24 h (light+dark)	[52]

Table 2 Single-phase long persistent luminescent catalysts for photocatalytic organic degradation

LPLs	Afterglow duration	Emission peak	Target pollutants	Degradation efficiency	Reference
$Zn_2SiO_4:Ga^{3+}$	30 min	398 nm	Permethrin	97%/2 h (light)	[53]
$Sr_2MgSi_2O_7:Eu^{2+},Dy^{3+}$ (Ag-loaded)	15 h	470 nm	Rhodamine B	88.9%/8 h (light)	[54]
			methylene blue	75.9%/8 h (light)	
			methyl orange	46.5%/8 h (light)	

The synthesis strategies for composite long persistent luminescent materials (LPLs) can be broadly categorized into physical mixing and chemical coupling. Early studies on the photocatalytic/electrocatalytic applications of composite LPLs predominantly adopted physical mixing. Li et al.[40] prepared a composite long-afterglow catalyst by mechanically blending $TiO_{2-x}N_y$ with $CaAl_2O_4:(Eu^+, Nd^+)$ *via* planetary ball milling. $CaAl_2O_4:(Eu^+, Nd^+)$ emits blue light at 440 nm, upon 325 nm UV excitation, while the nitrogen-doped TiO_2 extends its visible absorption band to 700 nm, resulting in effective spectral overlap between the two components. This enables the LPLs to act as a persistent light source for exciting the semiconductor. Under mercury lamp irradiation, the composite catalyst exhibited superior NO removal efficiency compared to pure $TiO_{2-x}N_y$. Moreover, it retained the ability to decompose NO for up to 3 h after light exposure ceases, demonstrating "light storage-controlled release catalysis" properties. This clearly demonstrates that "spectral matching" is the primary principle of in composite systems design, that is, the emission wavelength of the LPLMs must effectively overlap with the absorption band of the coupled semiconductor. However, simple mechanical mixing may result in poor interfacial contact, limiting the charge transfer efficiency. Li et al.[21] coupled a series of aluminate-based LPLMs, including $CaAl_2O_4:(Eu^+, Nd^+)$, $Sr_2MgSi_2O_7:Eu^+$, $Sr_4Al_{14}O_{25}:(Eu^+, Dy^+)$, $SrAl_2O_4:(Eu^+, Dy^+)$ and $SrAl_2O_4:Eu^+$, with $TiO_{2-x}N_y$ to systematically investigate the photocatalytic degradation performance of gaseous acetaldehyde pollutants in a closed system. The amount of CO_2 produced by the different composite catalysts varied significantly. The overall CO_2 yield followed the order: $CaAl_2O_4:(Eu^+, Nd^+) > Sr_2MgSi_2O_7:Eu^+ > Sr_4Al_{14}O_{25}:(Eu^+, Dy^+) > SrAl_2O_4:(Eu^+, Dy^+) > SrAl_2O_4:Eu^+$. This trend correlates with the afterglow wavelength of the respective LPLs. Among them, the most optimal $CaAl_2O_4:(Eu^+, Nd^+)$ exhibits the shortest emission peak at 440 nm, attributed to the $4f^6 5d \rightarrow 4f^7$ electronic transition of the Eu^+ ions. After 180 min of visible light irradiation, this system can completely degrad 1.161×10^{-3} of acetaldehyde, generating 1.642×10^{-3} of CO_2, corresponding to a mineralization rate of 70.7%. Although the initial luminescence intensity of $CaAl_2O_4:(Eu^+, Nd^+)$ was relatively low, its extended afterglow lifetime enabled it to sustain photo-assisted catalytic activity for more than 360 min after the light source was turned off, producing approximately 5.0×10^{-5} of CO_2. This study preliminarily revealed the crucial influence of the afterglow wavelength on photocatalytic efficiency.

Even within the same aluminate-based family, differences in the local crystal field environment of the Eu^+ emission centers and the distribution of trap energy levels can lead to variations in afterglow properties, thereby affecting their effectiveness as "built-in light sources" for catalytic assistance. Compared to $TiO_{2-x}N_y$ combined with LPLs materials, Ag_3PO_4-based photocatalysts demonstrate superior activity in degrading organic dyes. However, their application is limited by poor photostability due to the susceptibility of Ag^+ to photocorrosion[41]. To address this issue, Zhang et al.[42] deposited Pt nanoparticles onto the Ag_3PO_4 surface to promote the separation of photogenerated charges, while simultaneously blending the long persistent luminescent material $CaAl_2O_4$:Eu^+, Nd^+ with a silicone-acrylic emulsion to form a corrosion-resistant coating. This coating emits blue-violet long afterglow at 440 nm, overlapping with the absorption band of Pt/Ag_3PO_4. In a Rhodamine B (RhB) degradation experiment, the composite catalyst achieved an 81.7% degradation rate within 5 h, outperforming the 54.1% achieved by pure Ag_3PO_4 (54.1%) alone. In the dark, the RhB solution gradually faded in the presence of the composite catalyst, while a blank coating without LPLs showed no such degradation. During the daytime, $CaAl_2O_4$:Eu^+, Nd^+ absorbs sunlight, exciting Eu^+ and causing electron-hole separation. The electrons migrate through the conduction band and are trapped by VO^+ and $NdCa^+$ defects, later escaping due to thermal disturbance at room temperature and returning to the conduction band. Finally, they undergo radiative transitions back to the $4f^7$ ground state of Eu^+, simultaneously emitting 440 nm afterglow. This persistent luminescence further excites Pt/Ag_3PO_4 to generate electron-hole pairs and reactive species such as h^+ and $\cdot OH^-$, which oxidize and degrade dye molecules. Corrosion resistance tests confirmed that the diffraction peaks and 440 nm emission intensity of the $CaAl_2O_4$:Eu^+, Nd^+ coating remained stable after immersion, demonstrating that the silicone-acrylic emulsion strategy enhances chemical stability and shows promise in mitigating corrosion and degradation issues.

Havasi et al.[43] combined the long persistent luminescent material $Sr_4Al_{14}O_{25}$:Eu^+, Dy^+ (SRAL) with a ZnO:Co+Ag catalyst to construct a composite system. Using the degradation of methyl orange (MO) in aqueous solution as a model reaction, they systematically investigated the performance of various ZnO:Co+Ag/SRAL composites for energy-saving wastewater purification. ZnO:Co+Ag can utilize violet and blue light, while SRAL (emitting at 495 nm, blue-green) can provide photoluminescence assistance. The study employed two experimental setups to optimize the photocatalytic performance of the composite long-afterglow catalyst. One is the "SRAL-mixed" scheme, where the composite catalyst was placed directly in the reaction vessel. The other is the "PDMS/SRAL-assisted" scheme, where the catalyst was immobilized in a PDMS layer positioned beneath the transparent bottom of the reaction vessel. A catalyst without SRAL served as the control group, placed directly within the reaction vessel. The composite catalysts were tested under three distinct illumination modes: continuous light (210 min illumination, 0 energy saving), 1–1 s pulsed light (105 min illumination, 50% energy saving), and 1–10 s pulsed light (21 min illumination, 90% energy saving), as detailed in Figure 5 (a)[43]. The complete experimental procedure consisted of (1) different pre-illumination treatments of the LPLs; (2) photocatalytic reaction; (3) solution sampling; (4) determination of MO concentration by UV-vis spectrophotometry. The results (Figure 5(b)) showed that the photocatalytic activity followed the order: no LPL assistance < "PDMS/SRAL-assisted" scheme < "SRAL-mixed" scheme; and 1–10 s pulses < 1–1 s pulses < continuous illumination. Notably, the 1–1 s pulsed mode in the "SRAL-mixed" scheme achieved a degradation efficiency of 81% within 210 min, approaching the 83.6% degradation efficiency of pure ZnO:Co+Ag under continuous illumination. It is worth mentioning that although the 1–10 s pulsed mode has the shortest illumination time, it can still degrade over 60% of MO within 210 min. This indicated that the presence of SRAL can maintain relatively high catalytic efficiency while significantly reducing the required lighting power. Moreover, photocatalytic activity was also observed in darkness solely *via* the afterglow emission from pre-illuminated LPLs. As shown in Figure 5(c), increasing the SRAL content in the PDMS/SRAL plate (black squares) significantly enhanced catalyst performance, confirming that the visible light emitted by SRAL can effectively drive the photocatalytic reaction of ZnO:Co+Ag nanoparticles. Compared to the "PDMS/SRAL-assisted" scheme (black squares), the "SRAL-mixed" scheme (green pentagons) exhibits superior catalytic activity, achieving 77.9% MO degradation. Indeed, both assistance modes effectively promoted the photocatalytic dye degradation under continuous and pulsed illumination conditions. Nevertheless, the researchers in this paper recommended the "PDMS/SRAL-assisted" scheme for practical applications, as it avoids potential environmental and economic risks associated with the dissolution and separation of LPLs, as well as issues related to polarization or shielding effects.

$SrAl_2O_4$:Eu^+,Dy^+ (SAO) is one of the most classic aluminosilicate-based long persistent luminescent materials (LPLs). Lu et al.[44] designed a SAO-based Cu_2O nanocrystal/TiO_2 microsphere rotating-disk reactor. Compared to conventional fixed-bed systems, the rotating catalyst disk generates a continuously renewed thin water film, which shortens the light-path length, reduces solution light absorption, accelerates the refreshment of surface pollutants and their intermediates, and thereby enhances photocatalytic activity. The built-in SAO component absorbs excess light energy and produces long-lasting afterglow, exciting $Cu_2ONCs/M\text{-}TiO_2$ to generate photogenerated charge carriers, thereby enabling continuous catalysis without an external light source. This rotating disk reactor achieved 24 h, round-the-clock degradation rates of 98% for rhodamine B and 93% for bisphenol A. However, this study merely employed the LPL as an external auxiliary

light source and did not explore the potential intrinsic performance enhancement that could arise from its composite integration with other catalysts. Numerous studies have shown that SAO can be chemically integrated with various semiconductor materials to construct novel photocatalytic systems, particularly with g-C_3N_4. Aliabadi et al.[45] synthesized SAO *via* the gel-combustion method and integrated it with g-C_3N_4/WO_3/Bi_2WO_6 to construct a dual Z-scheme heterojunction photocatalyst. This composite increased the dye removal rate under illumination from 88% to 98%. Moreover, under weak light conditions (simulating cloudy weather), the composite still degraded 87% of the pollutant within 20 min. In another study, Li et al.[46] combined SAO with g-C_3N_4 through high-temperature calcination to fabricate a binary composite catalyst. This system achieved up to 80% degradation rate of basic fuchsin (BF) within 10 min, approaching complete degradation within 20 min. After the light source was removed, the composite maintained 90% BF degradation rate within 3 h, whereas pure g-C_3N_4 exhibited no catalytic activity. Interestingly, pure SAO exhibited higher degradation efficiency in the dark than the SAO/g-C_3N_4 composite, suggesting that the incorporation of g-C_3N_4 has a certain effect on the light absorption and energy storage of SAO. Mechanistic studies reveal that under visible-light irradiation, photogenerated electrons in the valence band of g-C_3N_4 are excited to its conduction band, leaving holes behind. Because the conduction band potential of SAO (+0.32 eV) is higher than that of g-C_3N_4 (−1.03 eV), electrons transfer from g-C_3N_4 to SAO. Simultaneously, holes reverse-migrate to g-C_3N_4, as the valence band potential of SAO (+2.47 eV) is higher than that of g-C_3N_4 (+1.65 eV). This bidirectional charge separation significantly enhances the separation efficiency of photogenerated carriers, boosting photocatalytic activity. In SAO, photoexcitation promotes Eu^+ from ground state ($4f^7$) to an excited state ($4f^6 5d$), oxidizing Eu^+ to Eu^+, while Dy^+ traps electrons and is reduced to Dy^+. Under illumination, conduction-band electrons react with O_2 to generate superoxide radicals, which synergize with holes to mineralize pollutants (e.g., BF) into H_2O and CO_2.

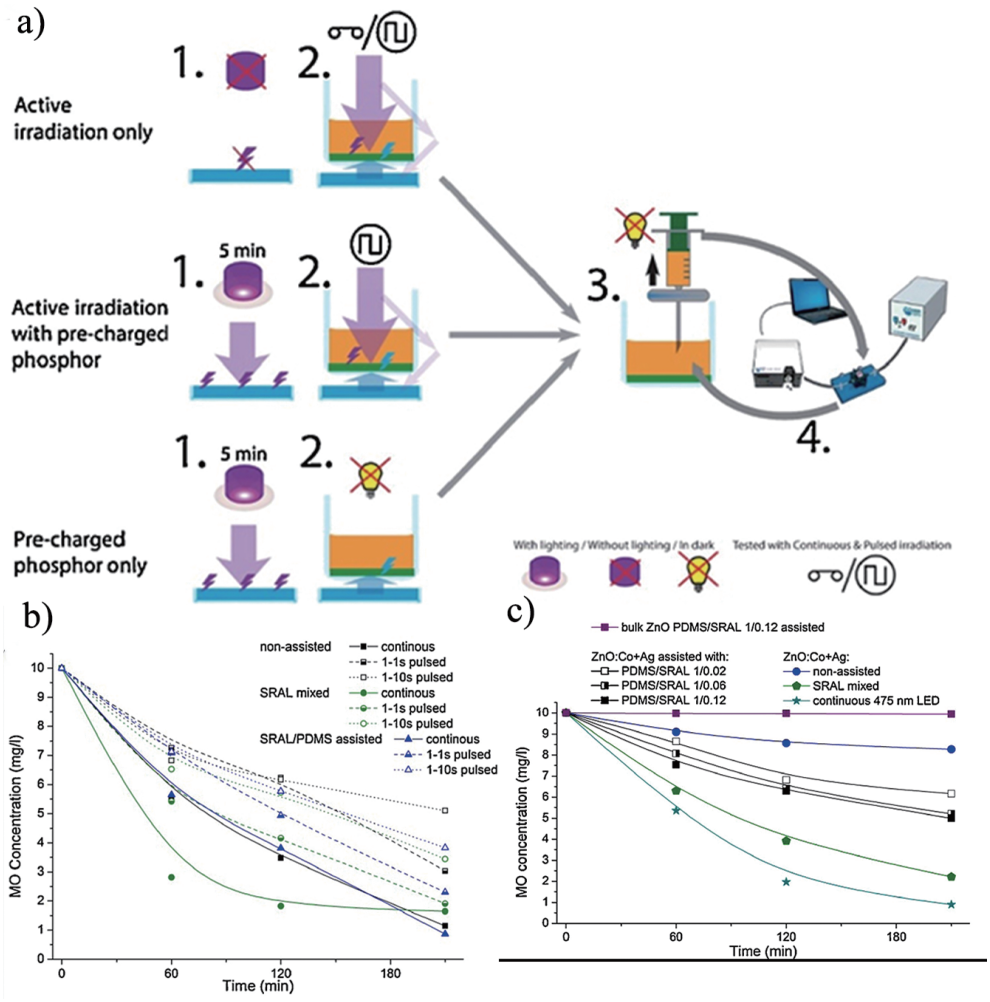


Fig. 5 (a) Overview of the illumination schemes; (b) Photodegradation performance of the catalyst under different schemes; (c) Degradation performance of the catalyst in the dark after pre-irradiation[43]
(with permission from Elsevier Publication)

In darkness, stored energy in SAO is released: Dy^+ releases electrons to the conduction band, which are transferred to Eu^+, reducing it back to Eu^+. Meanwhile, the afterglow excitation of SAO enables g-C_3N_4 to continuously generate active charge carriers, achieving long-term catalysis in dark environments. Another example is the work by Chen et al.[47] who constructed a dual Z-scheme ternary composite photocatalyst by integrating SAO with g-C_3N_4@NH_2-UiO-66 *via* a solvothermal method. Under 30 min of visible-light irradiation, this composite achieved a 95% degradation rate for methylene blue (MB), which is 5.86, 4.04 and 10 times higher than that of pure SAO, g-C_3N_4, and NH_2-UiO-66, respectively. Moreover, it maintained a 50% MB degradation rate over 5 h in the dark. While chemical integration generally leads to closer interfacial contact between LPLs and catalysts, the coupling does not always result in straightforward positive gains. Overall, composite catalysts tend to exhibit a lower band gap (E_g) and enhanced visible-light absorption capabilities.

Another commonly studied long persistent luminescent materials (LPLs) is the silicate-based $Sr_2MgSi_2O_7$:Eu^+,Dy^+ (SMSO). Bu et al.[48] constructed an SMSO/g-C_3N_4 Z-scheme heterojunction *via* mechanical mixing followed by sintering. Under visible-light irradiation, the composite catalyst achieved a 95% degradation rate of methylene blue within 30 min, with a reaction rate constant 3.2 times that of pure g-C_3N_4. Density functional theory calculations revealed that the Fermi levels of g-C_3N_4 and SMSO are –0.70 and –0.80 V (*vs.* NHE), respectively. The proposed mechanism involves the following steps: upon illumination, electrons in g-C_3N_4 are excited from the valence band (VB) to the conduction band (CB), while electrons in SMSO remain stable in its VB. Through the heterojunction interface, the photoexcited electrons in g-C_3N_4 transfer to the VB of SMSO and recombine with its holes. This process suppresses the recombination of electron-hole pairs in g-C_3N_4 itself, allowing holes in the VB of g-C_3N_4 (with strong oxidizing ability) and electrons in the CB of SMSO (with strong reducing ability) to accumulate, thereby synergistically enhancing the redox capacity of the system. Electron spin resonance (ESR) tests confirmed significantly enhanced signals of $\cdot O_2^-$ and ·OH radicals under light. In the dark, the material sustained catalytic activity for up to 5 h, achieving 50% degradation with a 32.6 times that pure g-C_3N_4. This is attributed to the spectral overlap between the photoluminescence peak of SMSO and the absorption spectrum of g-C_3N_4, enabling SMSO to persistently excite g-C_3N_4 in the absence of light, generate electron-hole pairs, and maintain charge separation through the Z-scheme interface to sustain the catalytic reactions.

Wu et al.[49] prepared SMSO *via* a solid-state method and combined it with Ag_3PO_4 using a solution mixing process. The absorption band of Ag_3PO_4 matches the 470 nm photoluminescence peak of SMSO originating from the Eu^+ ($4f^6 5d \rightarrow 4f^7$) transition. The loading of Ag_3PO_4, through the inner-filter and light-reabsorption effects, caused a 71%–83% attenuation in the PL intensity of SMSO (the quantum yield decreased from 7%–12% to about 2%) and weakened its afterglow. Nevertheless, the composite catalyst exhibited a 2.5-fold and 1.9-fold increase in photocatalytic efficiency for methyl orange (MO) under sunlight and visible light, respectivel. Moreover, residual MO was further degraded in the dark for 20 min after the light exposure ceased (reaching 32% and 9% degradation following solar and visible light excitation, respectively), whereas pure Ag_3PO_4 completely lost its degradation capability once illumination ceased. Ma et al.[50] fabricated a dual S-scheme heterojunction SMSO/$ZnIn_2S_4$/UiO-66-NH_2, *via* hydrothermal self-assembly method. The composite catalyst showed significantly higher degradation efficiencies for Rhodamine B (RhB) and methylene blue (MB) under visible light compared to its individual components, achieving degradation rates of 72.2% and 81.7% after 40 min (RhB) and 60 min (MB) irradiation, respectively. MB after 60 min of irradiation. After the light was turned off, the material continued to catalyze degradation in the dark *via* its afterglow for 4 h (RhB) and 6 h (MB), increasing the total degradation rates further to 86.7% and 96.8%, respectively.

In addition to aluminate- and silicate-based long persistent luminescent materials (LPLs), certain LPLs with other matrix compositions have also demonstrated excellent performance in photocatalytic degradation. Vaiano et al.[51] prepared nitrogen-doped TiO_2 (N-TiO_2) *via* a sol-gel method and combined it with a commercial blue-emitting LPL, $Sr_{2.90}Eu_{0.03}Dy_{0.07}Al_4SiO_{11}$ to construct a photocatalytic system driven by ultraviolet LEDs, aiming to reduce the energy consumption in photocatalytic wastewater treatment. The emission spectrum of this LPL (peak at 440 nm) can excite N-TiO_2, achieving a 90% decolorization efficiency for crystal violet through alternating light-dark cycles (total duration 60 min, actual illumination 30 min). In contrast, continuous illumination requires 60 min to attain the same efficiency. This strategy reduced energy consumption and economic cost by 42%.

He et al.[52] pioneered the covalent integration of ultralong-persistence phosphor (afterglow >16 d) with metal-organic framework, constructing, $Zn_3Ga_2Ge_2O_{10}$: 0.5%Mn/NH_2-MIL-101(Fe) (LPLs/MOFs) photocatalyst, significantly extended the timescale of dark-state catalysis from “hours” to “days,” greatly expanding the material’s potential for long-term catalytic applications. The study systematically compared two composite strategies—physical mixing and chemical bonding—demonstrating the significant advantages of the chemical approach in enhancing interfacial interactions and catalytic performance. This study utilized an aminosilane coupling agent to covalently modify hydrothermally synthesized LPLs onto the surface of NH_2-MIL-101(Fe), forming a heterojunction. The afterglow emission spectrum of the composite (peak at 535 nm) overlapped strongly with the absorption spectrum of the MOF, enabling an efficient persistent luminescence resonance energy transfer (PLRET) mechanism. After 120 min of UV irradiation, LPLs/MOF (1∶1) composite

completely degraded Rhodamine B (RhB), exhibiting significantly higher degradation efficiency than the physically mixed LPLs+MOF (1∶1) counterpart. This enhancement is attributed to the heterojunction formed *via* covalent bonding, which effectively suppresses the rapid recombination of photogenerated electron-hole pairs, while the high specific surface area of the MOF provides abundant active sites. After turning off the light following 30 min of irradiation, the composite continued to degrade RhB for up to 12 h, achieving a total degradation rate of 98% within 24 h. In contrast, the physically mixed system showed reduced PLRET efficiency due to excessive spacing between LPLs and MOFs.

2.2 Continuous photocatalytic degradation of organic pollutants driven by single-phase long persistent luminescent materials

Currently, numerous studies have explored photocatalytic systems based on long persistent luminescent materials (LPLs) to achieve persistent photocatalytic degradation of organic pollutants. However, most of these studies rely on combinations of two materials. Whether through physical blending or chemical coupling *via* heterojunction formation, the LPL component typically does not serve as the primary catalytic agent. Instead, it acts as a persistent light source for the coupled semiconductor catalyst, enabling continued activity in the dark. In contrast, single-phase LPLs can simultaneously exhibit both persistent luminescence and high catalytic efficiency. Consequently, the research focus is gradually shifting from composite systems to single-phase LPLs to explore their potential for direct photocatalytic degradation of organics. Relevant studies remain relatively limited. The following section introduces two distinct strategies for designing single-phase LPL catalysts: one focuses on "intrinsic modification" through bulk ion doping to tailor the material's native defects and energy-level structure, while the other employs "extrinsic modification" *via* surface nano-loading to introduce new optical and catalytic active sites. The former emphasizes structural homogeneity and stability, whereas the latter offers greater flexibility for integrating diverse functional nanomaterials.

Zhou et al.[53] developed a single-phase, "dual-functional" long persistent luminescent material (LPL) $Zn_2SiO_4:Ga^+$, which significantly extends the lifetime of photogenerated charge carriers by introducing positive charge traps through Ga^+ doping, solving the issue of insufficient light penetration depth in conventional photocatalysts under high-concentration conditions. The catalyst was synthesized *via* a sol-gel method with a Ga^+ doping concentration of 1% (atomic percent). Upon 254 nm UV excitation, $Zn_2SiO_4:Ga^+$ exhibits broad-band emission from 320 to 650 nm, featuring a main UV peak at 362 nm and a shoulder peak at 462 nm attributed to Ga^+ doping (Figure 6(a)). Its long persistent luminescence covers 325–550 nm, with a dominant peak at 398 nm, and the afterglow intensity is sufficient for naked-eye observation in the dark for over 5 min (Figure 6(b)). The decay curve of $Zn_2SiO_4:Ga^+$ follows a double-exponential model (fast decay constant τ_1 = 0.87 min, slow decay constant τ_2 = 4.30 min), with the afterglow signal remains detectable for over than 30 min, extending the charge-carrier separation lifetime to the minute scale (Figure 6(c)). In degradation tests using 10 mg/L permethrin, $Zn_2SiO_4:Ga^+$ (2 g/L) achieved a total organic carbon (TOC) removal rate of 97.1% under 2 h of UV irradiation, significantly higher than the 59.7% removal by undoped Zn_2SiO_4 (Figure 6(d), (e)). A key advantage of this material is its adaptability to high catalyst concentrations: even at 10 g/L, $Zn_2SiO_4:Ga^{3+}$; maintained a TOC removal efficiency of 97%, whereas conventional Zn_2SiO_4 dropped to 28%. This phenomenon is attributed to the positive charge traps formed by Ga^{3+} doping, which capture photogenerated electrons and suppress recombination. Simultaneously, the persistent luminescence enables the catalyst to transfer stored ultraviolet energy deep into the solution, overcoming light-scattering limitations in high-concentrated systems. Moreover, the catalyst showed stable performance across a pH value range of 5–9 and under various water conditions (pure water, tap water, saline water), with activity declining only from 92.1% to 88.6% after five cycles, demonstrating excellent reusability.

Hai et al.[54] systematically investigated the performance of the classic silicate long persistent luminescent material $Sr_2MgSi_2O_7:Eu^+,Dy^+$ (SMSO) in the degradation of persistent organic dyes. To enhance its catalytic efficiency, they uniformly loaded silver nanoparticles onto the material surface *via* a photochemical reduction method. Optically, SMSO exhibits an excitation spectrum ranging from 250 to 450 nm, with an emission peak at 470 nm. Afterglow testing revealed that the initial afterglow brightness of pristine SMSO was 700 mcd/m^2, while Ag-loaded SMSO increased remarkably to 6800 mcd/m^2 (an 871% enhancement), with an afterglow duration exceeding 15 h. In photocatalytic experiments, SMSO exhibited a degradation rate of 45.1% for Rhodamine B (RhB) after 8 h of UV irradiation. After the light was turned off, the degradation rate increased to 76.5% over the subsequent 24 h in the dark. Under the same 24 h period, SMSO also degraded methylene blue (MB) and methyl orange (MO) by 39.5% and 20.4%, respectively. After Ag modification, the degradation performance improved significantly: 88.9% for RhB, 75.9% for MB and 46.5% for MO. The variation in degradation efficiency among the dyes stems from their structural properties: the N^+ group in RhB is relatively susceptible to destruction, whereas the azo structure in MO is more stable. Furthermore, pH significantly influenced the degradation performance. The highest degradation rate for RhB (80.6%) occurred under acidic conditions, while optimal degradation for MO (40.2%) and MB (63.1%) was observed under alkaline conditions.

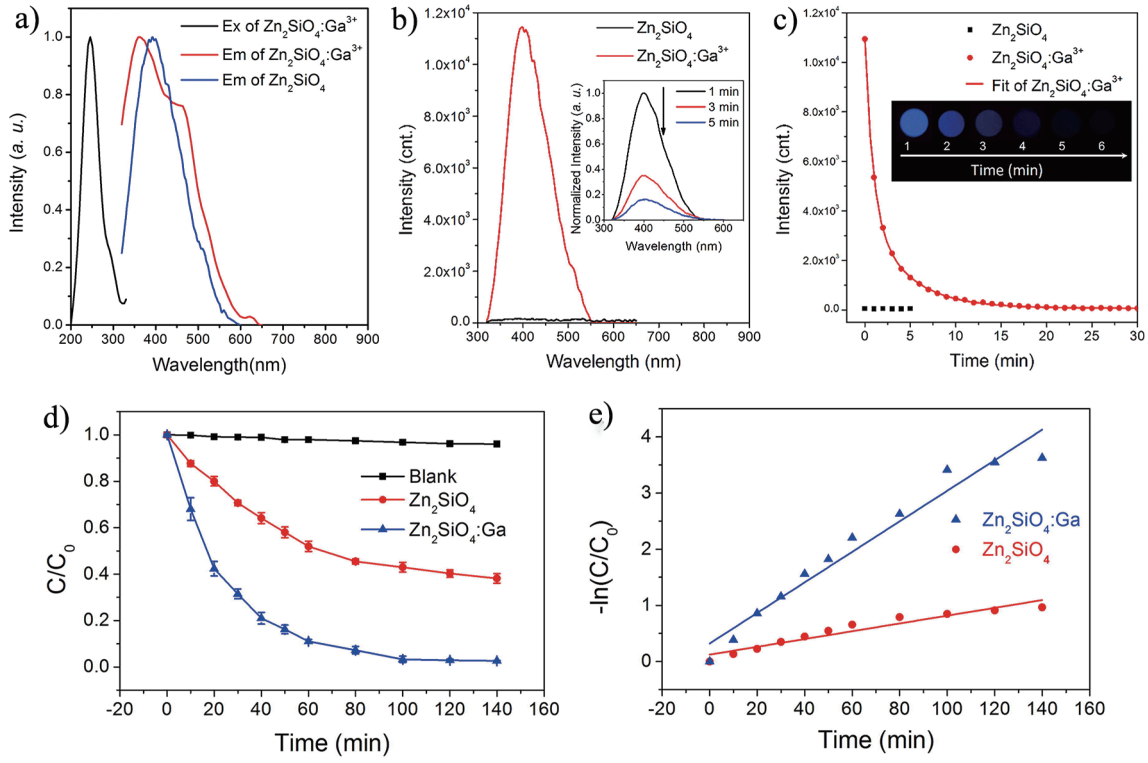


Fig. 6 (a) Photoluminescence of Zn_2SiO_4 and Zn_2SiO_4:Ga^{3+}; (b) Afterglow emission of Zn_2SiO_4:Ga^{3+}; (c) Afterglow decay curve of Zn_2SiO_4:Ga^{3+}; (d), (e) Photodegradation of permethrin under UV irradiation using Zn_2SiO_4 and Zn_2SiO_4:Ga^{3+}

Note: The inset in (b) shows the afterglow spectra of Zn_2SiO_4:Ga^{3+} at different time intervals, the inset in (c) shows a digital photograph of the Zn_2SiO_4:Ga^{3+} afterglow after cessation of excitation[53].

(with permission from Elsevier)

This behavior is correlated with the generation efficiency of radicals (·OH) and the dye adsorption capacity. Mechanistic studies indicated that under illumination, Eu^+ excitation generates electron-hole pairs, with some electrons being captured by Dy^+. In the dark, the gradual release of electrons from these trap levels sustains the catalytic reaction. Ag nanoparticles enhanced light absorption capacity through surface plasmon resonance effect while promoting interfacial electron migration, effectively inhibiting electron-hole pair recombination.

3 Long persistent luminescent materials enabling continuous photocatalytic hydrogen evolution

Hydrogen, as a clean and renewable energy source with high energy density, holds great promise for replacing traditional non-renewable fuels[55]. However, its high flammability, explosiveness, and its hydrogen embrittlement effect on metals pose significant challenges for safe storage and transportation[56]. Photocatalytic hydrogen production offers a potential solution to these issues. Unfortunately, current systems suffer from low efficiency and practical limitations, calling for novel materials or technological advances for improvement[57]. The progress of long persistent luminescent materials (LPLs) in photocatalytic degradation has naturally spurred interest in applying them to clean energy production, particularly in photocatalytic hydrogen evolution[58]. Similar to the strategies used in degradation, the approaches here can also be divided into composite systems and single-phase systems (Tables 3 and 4). To systematically outline developments in this field—consistent with the earlier discussion on photocatalytic organic degradation—the following sections will summarize relevant studies based on the type of LPL host matrix, presented in chronological order.

3.1 Composite long persistent luminescent materials for achieving continuous

Currently, composite long-afterglow materials applied to photocatalytic water splitting for hydrogen evolution primarily rely on heterojunctions constructed through chemical coupling strategies. Liu et al.[59] successfully fabricated a g-C_3N_4@Au@$SrAl_2O_4$:Eu^+,Dy^+ composite catalyst using a Pechini-type sol-gel method combined with mechanical mixing and high-temperature calcination.In this system, the afterglow emission spectrum of $SrAl_2O_4$:Eu^+,Dy^+ (SAO, 450–600 nm) shows strong overlap with the absorption spectrum of g-C_3N_4@Au, while Au nanoparticles enhance visible-light absorption through surface plasmon resonance.

Table 3 Composite long persistent luminescent catalysts for photocatalytic hydrogen evolution *via* water splitting

LPLs	Catalysts	Emission peak	Hydrogen production	Reference
$SrAl_2O_4:Eu^{2+},Dy^{3+}$	g-C_3N_4@Au	510 nm	987 μmol/(g·h) (light)	[59]
	Cu|CuO	450–600 nm	96.04 μmol/(g·h) (light+dark)	[60]
$Sr_2MgSi_2O_7:Eu^{2+},Dy^{3+}$	Ag_3PO_4	470 nm	491 μmol/(g·h) (light) 33.33 μmol/(g·h) (dark)	[61]
	CdS	470 nm	36140 μmol/(g·h) (light) 1577.5 μmol/(g·h) (dark)	[63]
$Sr_2MgSi_2O_7:Eu^{2+},Dy^{3+}$ (Ag-loaded)	$BiFeO_3$/Ag	430−600 nm	111.16 μmol/(g·h) (light) 14.27 μmol/(g·h) (dark)	[62]
$ZnGa_5Si_5O_{18}$	SCN	500 nm	3963.80 μmol/(g·h) (light)	[64]
$Zn_2GeO_4:Mn^{2+},Li^{+}$	COFs		35000 μmol/(g·h) (light)	[65]

Table 4 Single-phase long persistent luminescent catalysts for photocatalytic hydrogen evolution *via* water splitting

LPLs	Afterglow duration	Emission peak	Hydrogen production	Reference
$Sr_2MgSi_2O_7:Eu^{2+},Dy^{3+}$	20 h	465 nm	14000 μmol/(g·h) (light) 33 μmol/(g·h) (dark)	[66]
$Sr_2MgSi_2O_7:Eu^{2+},Ce^{3+}$	8 h	467 nm	13,000 μmol/(g·h) (light) 93.8 μmol/(g·h) (dark)	[68]

Under visible-light irradiation, the order of hydrogen evolution activity was: g-C_3N_4@Au@SAO > g-C_3N_4@SAO > g-C_3N_4@Au > g-C_3N_4. After the light was turned off, only g-C_3N_4@Au@SAO maintained hydrogen evolution activity. This work first demonstrated photocatalytic hydrogen evolution in an aqueous phase using a composite LPL material. Tu et al.[60] coupled SAO with Cu|CuO *via* an incomplete solid-state reaction to fabricate a Z-scheme heterojunction Cu|CuO/SAO composite film photocatalyst. This material utilizes the green afterglow emitted by SAO in the dark to excite CuO and generate photogenerated charge carriers. XRD and SEM characterization revealed that a tight Z-scheme heterojunction formed between fibrous CuO (~200–300 nm) and SAO particles (~1000–1500 nm), which helps suppress electron-hole recombination and thereby enhances the redox capability of the material. The total hydrogen production of the composite film reached 672.29 μmol/g over 180 min of simulated sunlight irradiation followed by 240 min in darkness.

$Sr_2MgSi_2O_7:Eu^{+},Dy^{+}$ (SMSO), a classic silicate-based long persistent luminescent material (LPL), has also garnered significant attention for photocatalytic hydrogen evolution. Tang et al.[61] constructed a novel Z-scheme composite SMSO/Ag_3PO_4 *via* a solvent-based method for hydrogen production. Experimental results showed that the composite photocatalyst with a mass ratio of 15∶1 between SMSO and Ag_3PO_4 exhibits, producing 491 μmol/g of H_2 after 1 h of simulated sunlight irradiation. The hydrogen yield further increased by 100 μmol/g over 3 h in the dark, reaching a cumulative total of 591 μmol/g. In a separate study, Tang et al.[62] built a Z-scheme photocatalytic system by integrating SMSO with $BiFeO_3$ and further enhancing its performance with silver nanoparticles (Ag NPs). Herein, $BiFeO_3$ was synthesized *via* the hydrothermal method, while Ag NPs were deposited on SMSO *via* photoreduction, followed by the construction of a $BiFeO_3$/Ag/SMSO/Ag composite through sequential ionic layer adsorption, isoelectric precipitation, and high-temperature calcination. The loading of Ag NPs significantly boosted the luminescence intensity of SMSO and improved the sustained catalytic activity of the entire system. This catalyst achieved a hydrogen production of 444.64 μmol/g after 240 min of light irradiation—3.63 times that of bare $BiFeO_3$. Moreover, it produced an additional 57.07 μmol/g of H_2 during a subsequent 240 min dark period, representing a 3.15-fold improvement over the single-component catalyst. Wang et al.[63] employed a solvothermal method to fabricate a Type-II heterojunction composite photocatalyst by coupling SMSO with CdS (SMSO@CdS). Under UV-vis irradiation for 0.5 h, this material exhibited a remarkably high hydrogen evolution rate of 18.07 mmol/g, which is 326 times and 1.9 times that of pure SMSO and CdS, respectively (Figure 7(a)). In the dark, the composite continued to produce hydrogen for 4 h, with a cumulative yield of 6.31 mmol/g (Figure 7(b)), significantly outperforming both individual components (SMSO and CdS) and most reported counterparts. The superior performance of this system can be attributed to three key factors: (1) the heterojunction structure effectively

suppresses the recombination of photo-generated electron-hole pairs; (2) the afterglow emission of SMSO (peaking at 470 nm) overlaps well with the absorption band of CdS, enabling hydrogen production even without light; (3) the intrinsic electric field (IEF) interface synergistic effect and electron redistribution guides the directional migration of charges. Under dark conditions, electrons released thermally from Dy^+ traps are continuously transferred to the surface of CdS *via* the IEF to participate in hydrogen evolution (Figure 7(c)).

Through a solvothermal-calcination process, Abulimiti et al.[64] combined another silicate-based long-afterglow material, $ZnGa_5Si_5O_{18}$ (ZGSO), with sulfur-doped carbon nitride (SCN). Under xenon lamp irradiation, the ZGSO/SCN (1∶1) composite catalyst achieved a photocatalytic hydrogen evolution rate of 3963.80 μmol/(g·h), which is about 15 times higher than that of pure ZGSO (307.1 μmol/(g·h)) and 1.4 times higher than that of pure SCN (2800.80 μmol/(g·h)). Li et al.[65] employed a strategy of *in situ* growing covalent organic framework (COF) on the surface of Zn_2GeO_4:Mn^+, Li^+ (ZGO) LPLs to construct a core-shell heterojunction composite catalyst (ZGO@COF).

ZGO exhibits an emission peak at 540 nm, originating from the $^4T_1(^4G) \rightarrow {}^6A_1(^6S)$ electronic transition of Mn^+ ions. Its emission spectrum highly matches the absorption spectrum of the COF (Figure 8(a))[65], indicating that the afterglow luminescence from ZGSO can be effectively absorbed by the COF, thereby sustaining photocatalytic reactions even after light cessation. Photocatalytic performance testing revealed that ZGO@COF (1∶6) exhibited higher hydrogen evolution activity (Figure 8(b)) than pure COF (26.97 mmol/(h·g)) and pure LPLs (0.38 mmol/(h·g)). However, ZGO itself showed very weak hydrogen evolution performance, primarily due to its narrow light absorption range.

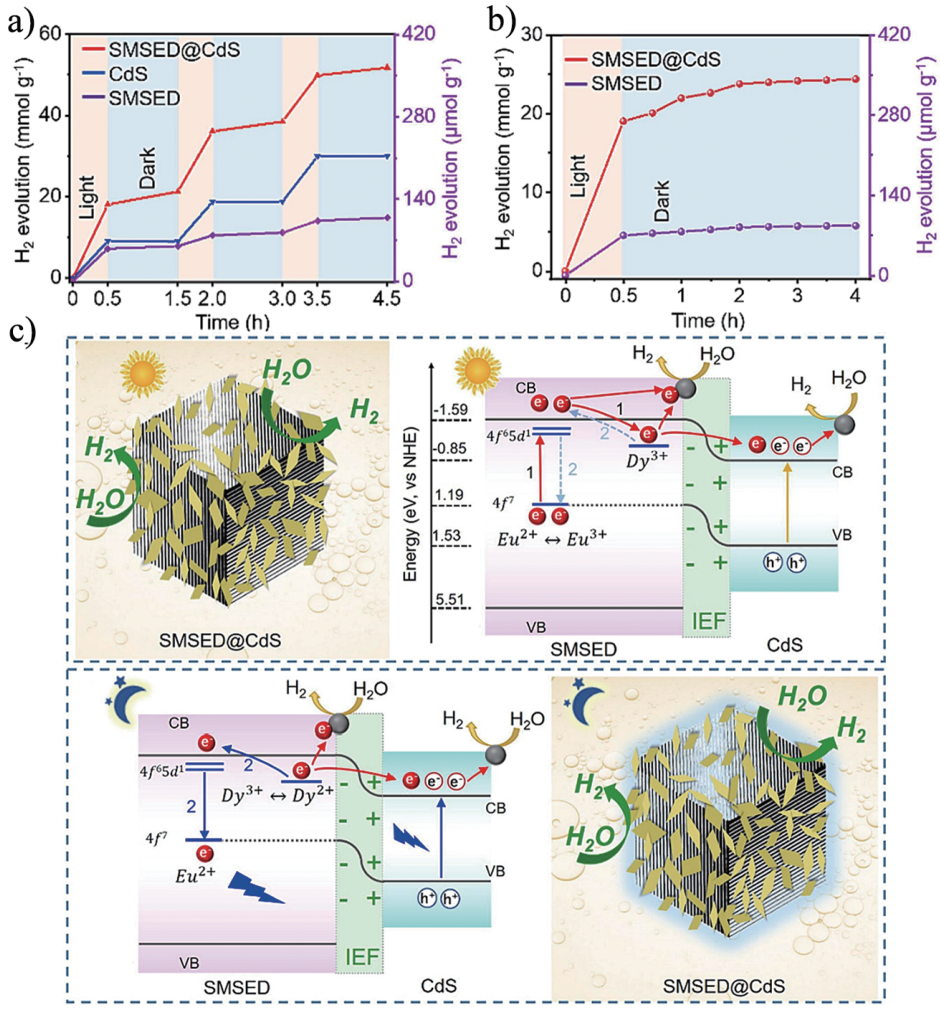


Fig. 7 (a) Hydrogen production yields of SMSO, CdS and SMSO@CdS; (b) Time course of hydrogen production for SMSO and SMSO@CdS after 0.5 h of UV-vis irradiation; (c) Proposed charge transfer mechanism for photocatalytic hydrogen production over SMSO@CdS under both illumination and dark conditions[63]
(with permission from Elsevier Publication)

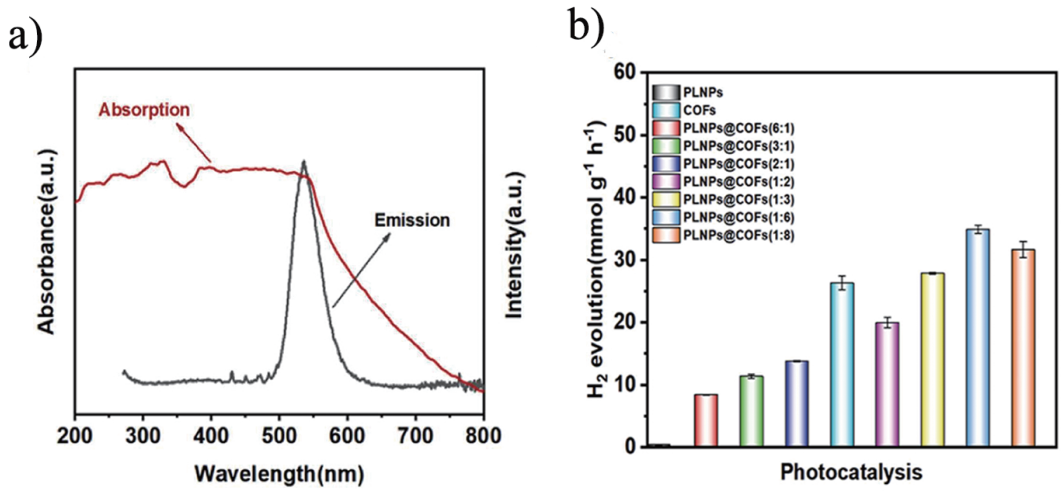


Fig. 8 (a) UV-vis diffuse reflectance spectra of COF and afterglow emission spectra of ZGO; (b) Photocatalytic H_2 evolution activity of the composite catalyst[65]
(with permission from Royal Society of Chemistry)

3.2 Single-phase long persistent luminescent materials for sustained photocatalytic hydrogen evolution

Unlike the research approach of composite long persistent luminescent materials (LPLs) in photocatalysis, which follows a "degradation-then-hydrogen evolution" pathway, studies on single-phase LPL catalysts for hydrogen evolution actually predate their exploration for organic degradation. Cui et al.[66] were the first to propose using a single-phase LPL directly as a photocatalyst to enhance light energy utilization efficiency. They synthesized $Sr_2MgSi_2O_7$:Eu^+,Dy^+ *via* a sol-gel method and systematically investigated its structure and properties. The results indicated that rare-earth ion doping induced oxygen vacancies and numerous lattice defects on the material surface, thereby enhancing photocatalytic activity. Eu^+ and Dy^+ introduced dopant energy levels within the forbidden band of $Sr_2MgSi_2O_7$, reducing its absorption bandgap from the intrinsic value of 7.9 to 2.34 eV. The valence band top and conduction band bottom of $Sr_2MgSi_2O_7$:Eu^+,Dy^+ were located at −1.44 eV, while the intermediate state formed by Eu^+ was positioned at 1.58 eV, with the intrinsic valence band of the host at 6.46 eV. This band structure meets the potential requirements for the hydrogen evolution reaction. Furthermore, the material exhibited long persistent luminescence with a maximum emission peak at 465 nm following UV excitation, persisting for over 20 h. Photocurrent measurements further confirmed its favorable photoelectric response characteristics. Evaluated its hydrogen evolution performance *via* methanol–water reforming under UV light, visible light, and dark conditions. When irradiated with a 500 W high-pressure mercury lamp (peak emission at 365 nm), $Sr_2MgSi_2O_7$:Eu^+,Dy^+ achieved a maximum hydrogen production rate of 14 mmol/(h·g), with a solar-to-hydrogen (STH) conversion efficiency of 5.18%—one of the highest light-energy conversion efficiencies reported in the field of photocatalytic hydrogen evolution at the time. After 15 min of UV exposure, hydrogen production continued to increase over time in the dark, reaching a cumulative 264 μmol/g after 8 h, with an STH conversion efficiency of 0.39% (Figure 9(a)). The possible mechanism reveals (Figure 9(b)) that under illumination, electrons in the ground state 4*f* of Eu^+ are excited to the 5*d* level, then thermally excited into the conduction band of $Sr_2MgSi_2O_7$, while Eu^+ is oxidized to Eu^+ by losing electrons. Most of the excited electrons originating from Eu^+ in the conduction band can directly interact with the reaction substrate, improving catalytic efficiency during illumination. Unconsumed electrons can be temporarily stored by Dy^+ ions, which are reduced to Dy^+, thereby prolonging the carrier lifetime (pathway I, indicated by red arrows in Figure 9(b)). In the dark, influenced by thermal disturbances, electrons are released from Dy^+ and continue to participate in the reaction, enabling sustained hydrogen production.

Previous studies have shown that when the sum of 4*f* electron counts of two different trivalent rare-earth ions is an integer multiple of 7 (e.g., Ce^+ (4*f*) and Eu^+ ($4f^6$)), a conjugated electronic structure can form. This enhanced electron transfer and light absorption in long persistent luminescent materials (LPLs)[67]. Fan et al.[68] first synthesized an LPL $Sr_2MgSi_2O_7$:Eu,Ce, with such a conjugated electronic structure *via* a sol-gel method and applied it to photocatalytic hydrogen evolution (HER) and oxygen evolution reactions (OER). The material exhibited a main emission peak in the blue region at 467 nm, with afterglow lasting over 8 h (Figure 10(a)). The introduction of Eu^+ and Ce^+ ions created intermediate energy levels, resulting in a band gap of 2.67 eV—significantly narrower than that of the undoped host (estimated from the absorption edge in Figure 10(b))[68]. Ultraviolet photoelectron spectroscopy (Figure 10(c)) revealed an intermediate state (acting as a valence band) at 2.82 eV, compared to the intrinsic valence band of the $Sr_2MgSi_2O_7$ host at 6.46 eV.

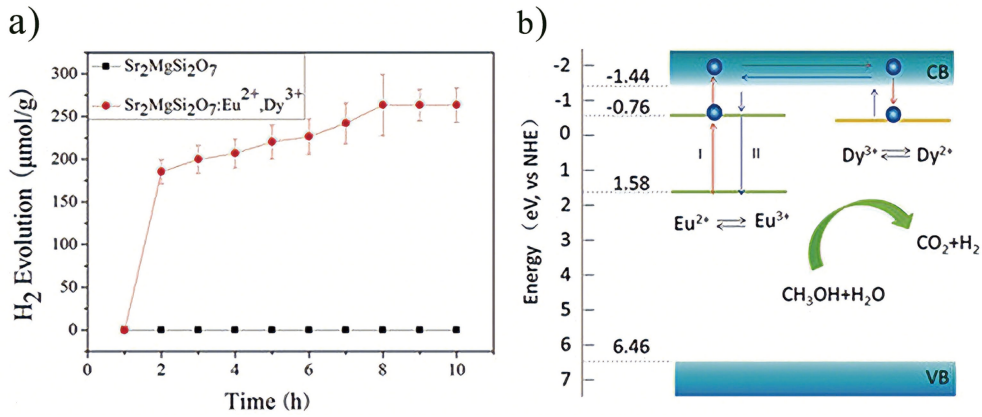


Fig. 9 (a) Time course of hydrogen evolution in the dark for $Sr_2MgSi_2O_7:Eu^{2+},Dy^{3+}$ and $Sr_2MgSi_2O_7$ after irradiation by a 500 W high-pressure mercury lamp for 15 min; (b) Schematic diagram of energy levels and the photoinduced electron transfer process[66] (with permission from Wiley-VCH)

Considering the critical role of the host's intrinsic conduction band in transferring photogenerated electrons for afterglow, the energy level at −1.44 eV was assigned as the conduction band minimum of $Sr_2MgSi_2O_7$:Eu,Ce. Under irradiation from a 500 W mercury lamp, the hydrogen and oxygen evolution rates reached 13.0 and 0.67 mmol/(g·h), respectively (Figure 10(d), (e)). More notably, after 2 h of UV pre-irradiation and subsequent placement in the dark, the material continued to produce hydrogen and oxygen, accumulating 0.75 mmol/g of H_2 and 2.34 mmol/g of O_2 over 8 h (Figure 10(f), (g)). Compared to $Sr_2MgSi_2O_7$:Eu and $Sr_2MgSi_2O_7$:Ce, the co-doped $Sr_2MgSi_2O_7$:Eu,Ce demonstrated superior photocatalytic efficiency under both light and dark conditions, indicating that the coexistence of Eu and Ce is crucial for achieving efficient water splitting, particularly for the OER half-reaction. In $Sr_2MgSi_2O_7$:Eu,Ce, oxygen vacancy defects serve as the primary electron traps, Eu^+ acts as the luminescent center, and Ce^+ functions as a photosensitizer that enhances Eu^+ emission *via* energy transfer. As illustrated in Figure 10(h), under illumination, 4 *f* electrons of Eu^+ are excited to the conduction band of the host and participate directly in reactions. The remaining unexhausted excited electrons are captured by electron traps and released slowly to interact with reactants (Path I). Simultaneously, excited electrons generated from Ce^+ absorption follow two competitive transfer paths (Path II), both contributing to enhanced catalytic efficiency: (1) they can be captured by electron traps or directly transferred to Eu^+, to form Ce^{4+}, oxidizing surface OH^- to produce oxygen. (This is enabled by the facile electron transfer between Eu^+ and Ce^+ within the conjugated structure, leading to the anomalous valence states Ce^{4+} and Eu^+). (2) Excited electrons can relax to the ground state, with the released energy being absorbed by Eu^+, thereby increasing the number of photogenerated carriers from Eu^+ and reducing non-radiative losses (Path II). XPS analysis (Figure 10(i), (j)) confirmed the coexistence of Ce^+, Ce^{4+}, Eu^+ and Eu^+, indicating a dynamic valence equilibrium and charge transfer within the system. This conjugated structure promotes charge transfer between active sites and improves the efficiency of the catalytic cycle. Although the material's band structure satisfies the thermodynamic requirements for overall water splitting, the strong association of Ce^+ with lattice-oxygen migration significantly enhances oxygen evolution capability. This leads to a mismatch between HER and OER rates, making it difficult to achieve simultaneous, efficient overall water splitting. This study provides a novel perspective for designing high-performance long-persistent photocatalysts based on conjugated electronic structures.

4 Long persistent luminescent materials powering photovoltaic cell for all-weather power generation

With the accelerated global energy transition, renewable energy has emerged as a core solution for addressing climate change and energy pollution due to its environmental friendliness and sustainability. Among renewable sources, solar energy holds a dominant position owing to its virtually inexhaustible supply and zero-carbon emission advantages. Photovoltaic technology, based on the photovoltaic effect in a semiconductor, efficiently converts solar radiation into electrical energy[69]. As typical photoelectric devices, solar cells rely on a series of charge-transfer processes—including the generation, separation, and transport of photo-generated carriers—for energy conversion. Although the technology has evolved through three generations, maintaining efficient power conversion under dark or low-light conditions remains a significant challenge[70]. A promising approach currently involves constructing a light-storage-release synergistic mechanism: storing the energy of unabsorbed photons in the photoanode material during illumination and exciting its sustained release under dark conditions. Long persistent luminescent materials (LPLs), as novel optical energy-storage materials, can capture and release light energy with delayed release across multiple bands from ultraviolet to infrared. By incorporating composite photoanodes using LPLs, they serve both as temporary light-energy reservoirs and as supporting structures for light absorbers. This dual-function design enables solar cells to maintain high efficiency during

daylight while also providing continuous power generation capability in dark environments[19]. Current research in this area mainly follows two strategies: direct composite integration and separated spectral conversion.

The direct composite integration strategy aims to incorporate long persistent luminescent materials (LPLs) as a functional layer directly into the photoanode of solar cells. Early exploration in this direction was conducted by Sun et al.[71] Combined $SrAl_2O_4$:Eu,Dy (SAO) with a transparent TiO_2 layer and loaded CdS quantum dots *via* microwave-assisted chemical bath deposition to fabricate CdS quantum dot-sensitized solar cells (QDSSCs). The incorporation of SAO enhanced the cell conversion efficiency from 0.98% to 1.24% under one sun illumination (AM 1.5G, 100 mW/cm^2), primarily due to SAO's light-scattering and down-conversion effects (PL emission peak at 512 nm). After the light was turned off, the cell maintained a dark-state efficiency of 0.07% (corresponding to J_{sc} = 0.10 mA/cm^2, V_{oc} = 0.17 V) through the persistent afterglow mechanism of SAO, in which Dy^+ acts as a hole trap and continuously releases holes to Eu^+. Electrochemical impedance spectroscopy further indicated that the SAO layer reduced electron transport resistance and suppressed carrier recombination. Thus, SAO played a dual role: during illumination, its light-scattering and down-conversion effects improved light-harvesting and boosted the visible-light conversion efficiency; in the dark, its stored green afterglow continuously excited the quantum dots, enabling weak dark-state power generation. This work demonstrated the feasibility of direct integration of LPLs into photovoltaic devices, albeit with a very low dark-state efficiency. In subsequent research, Sun et al.[72] introduced SAO into CdSe quantum dot-sensitized solar cells. Compared to CdS, CdSe possesses a narrower bandgap (1.7 *vs.* 2.4 eV), enabling more effective absorption of SAO's down-converted light and broadening the light-harvesting range. Under AM 1.5G illumination, the cell efficiency increased from 0.82% to 1.22%, representing a 48% enhancement. The IPCE curve exhibited a dual-peak profile (350 and 500 nm), corresponding to the down-conversion emission and light-scattering contribution of the LPLs, respectively. After switching off the light following 1 min illumination, the cell retained a dark-state conversion efficiency of 0.04% (J_{sc} = 0.13 mA/cm^2, V_{oc} = 0.14 V), with a quantum efficiency as high as 78%. Deng et al.[73] introduced multi-color LPL layers (green, blue, and red) into a CdS/CdSe co-sensitized QDSSC, fabricating a TiO_2/QDs/LPLs composite photoanode *via* a doctor-blade method for the first time. Compared to the earlier single CdS or CdSe systems studied by Sun's group, this work employed a co-sensitization strategy to broaden the spectral response and optimized the integration of LPLs. The LPL layer (40 μm thick) was directly coated onto an TiO_2 film (18 μm thick) to extend the optical path through reflection and to enhance light harvesting *via* the down-conversion effect of LPLs (absorbing UV light <450 nm and emitting at 574 nm). With the green LPLs, the cell efficiency increased from 4.08% to 5.07% (a 24% improvement), the short-circuit current density (J_{sc}) rose from 12.89 to 15.36 mA/cm^2, and the IPCE peak reached 66%. These improvements primarily enhance efficiency under illumination, while no significant breakthroughs were achieved in dark-state power generation capacity.

Tang et al.[74] developed an all-weather solar cell based on a green-emitting long persistent luminescent material (LPL) and carbon quantum dots (CQDs). Using a rapid hydrothermal method, they converted carbohydrate precursors (e.g., glucose, maltol, and sucrose) into CQDs and combined them with LPLs to construct a photoanode (*m*-TiO_2/LPLs). The cell exhibits a layered structure. Under illumination (AM1.5, 100 mW/cm^2), the efficiency of CQD cells based on different carbon sources ranged from 0.11% to 0.17%. In the dark, the LPLs emitted stored light energy as green afterglow (centered at 505–515 nm) to excite the CQDs to generate current. Among these, CQDs derived from maltol achieved an efficiency of 15.1% under dark conditions. The afterglow intensity of the LPLs dropped rapidly from 58.8 to 2.7 μW/cm^2 within 100 s, yet sustained luminescence for up to 6 h. Correspondingly, in the dark, the maximum power density of the cell declined markedly from 8.535 to 0.419 μW/cm^2 within 2 h. This design ingeniously separates "energy storage" from "luminescence-absorption," enabling secondary spectral conversion and utilization. However, the extremely low absolute power output, coupled with the inherent limitations in carrier separation and transport efficiency of CQDs themselves, leaves this system still far from practical application.

In contrast, the decoupled spectral conversion strategy adopts a more pragmatic and flexible technical approach. Hu et al.[75] synthesized a specialized long persistent luminescent material, $Zn_3Ga_{1.975}Ge_2O_{10}$:1.0Cr^+, 1.0Yb^+, 0.5Er^+, capable of emitting near-infrared afterglow (700–850 nm). Under 980 nm laser excitation, the Yb^+-Er^+ pair generates upconversion luminescence at 525–660 nm, while the Cr^+ ions produce the 700–850 nm NIR afterglow. This afterglow spectrum aligns well with the spectral response range (600–1100 nm) of silicon solar cells. The physically separated "pivot-type" structure employs long-afterglow materials as independent embedded light sources to illuminate silicon cells in dark conditions. Although this design sacrifices integration, it offers a distinct advantage: it completely avoids interfering with the original cell's high-efficiency structure and operating mechanism, thereby avoiding issues such as interfacial recombination or increased resistance that could arise from direct composite integration. Experimental results demonstrated that, in complete darkness, the silicon cell achieved a maximum instantaneous conversion efficiency of 2.549%, with an average efficiency of 0.238% over 300 s, sustaining power generation for 8 h (J_{sc} = 4.88 μA/cm^2, V_{oc} = 0.914 mV). This research offers a novel approach for operating silicon solar cells under dark conditions, overcoming the limitation that traditional long-afterglow materials are confined to the visible light spectrum and significantly enhancing their potential application value. Nevertheless, the overall energy conversion efficiency remains relatively low; improving the quantum efficiency and energy density of the LPLs themselves may be the key to future advancements.

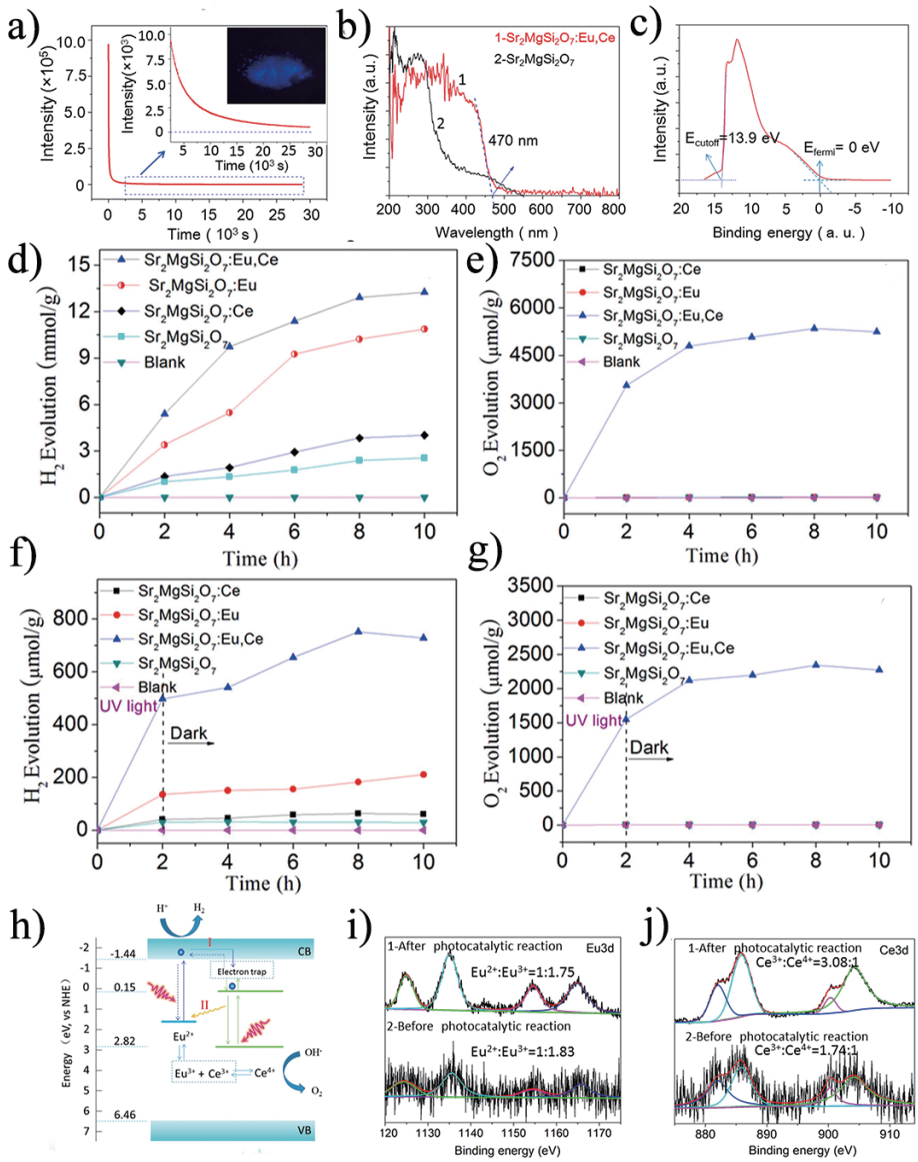


Fig. 10 (a) Luminescence and decay curves of $Sr_2MgSi_2O_7$:Eu,Ce; (b) UV-vis absorption spectra; (c) Ultraviolet photoelectron spectroscopy (UPS); (d)–(g): Hydrogen evolution amount (d) and oxygen evolution amount (e) under UV light irradiation, and hydrogen evolution amount (f) and oxygen evolution amount (g) in the dark, for $Sr_2MgSi_2O_7$:Eu,Ce, $Sr_2MgSi_2O_7$:Eu, $Sr_2MgSi_2O_7$:Ce, $Sr_2MgSi_2O_7$, and a blank solution; (h) Schematic diagram of photogenerated electrons and energy transfer process; (i) XPS spectra of Eu 3*d* before and after the photocatalytic reaction; (j) XPS spectra of Ce 3*d* before and after the photocatalytic reaction[68] (with permission from ACS Publications)

5 Long persistent luminescent materials-enabled around-the-clock photocatalytic CO_2 reduction and sterilization

The application of long persistent luminescent materials (LPLs) in photo-/electrocatalysis extends beyond pollutant degradation, water splitting for hydrogen production, and photovoltaic cells, with emerging exploration in areas such as solar fuel synthesis (e.g., CO_2 reduction) and environmental disinfection (e.g., photocatalytic sterilization). In the context of CO_2 reduction, the work by Pei et al.[18] is particularly instructive. Instead of constructing a heterojunction, they revisited the classic silicate LPL, $Sr_2MgSi_2O_7$:Eu^+,Dy^+ (SMSO), and applied a refined post-treatment process—high-temperature reduction—to engineer oxygen vacancies. The base material was synthesized *via* a sol-gel method followed by calcination at 900–1250 °C, and then subjected to a secondary high-temperature reduction treatment (e.g., 900 °C for 3 h) to tune the oxygen vacancy concentration. Oxygen vacancies serve a dual function, on one hand, they act as catalytic active sites, modifying the surface electronic structure to enhance the adsorption and activation of CO_2 molecules (the bond dissociation energy of C=O reaches 750 kJ/mol). On the other hand, they serve as electron storage-release centers: under illumination, trapping unconsumed photogenerated electrons under illumination

and suppressing electron-hole recombination. In the dark, the trapped electrons are slowly released *via* thermal stimulation, continuously driving CO_2 reduction for over 3 h. CO_2 reduction experiments showed that under illumination, the modified system achieved a significantly higher CO yield than the unmodified one. After the light was turned off, the modified material still maintained a measurable CO production rate, whereas the conventional material showed no activity. This work provides a model for designing single-phase long-afterglow catalytic materials, demonstrating that targeted defect engineering can integrate energy-storage centers with catalytic active sites, thereby simplifying the system and improving stability. However, the long-term stability of oxygen vacancies remains challenging under practical reaction conditions, particularly in environments containing water and oxygen.

In the field of photocatalytic sterilization, Zhang et al.[76] demonstrated the powerful potential of composite long-afterglow systems for functional customization. They achieved *in situ* composite construction of a $ZnIn_2S_4$ (ZIS)/$Sr_2MgSi_2O_7$:Eu^+,Dy^+ (SMSO) composite catalyst (ZIS/SMSO) featuring an S-type heterojunction structure. During the illumination period, the ZIS/SMSO heterojunction follows an S-scheme electron transfer pathway, effectively promoting the separation of photogenerated carriers while preserving the strong reduction capability of ZIS and the high oxidation capability of SMSO, thereby enhancing radical production. Electrons on the ZIS conduction band can reduce O_2 to form superoxide radicals ($\cdot O_2^-$), while holes in the SMSO valence band can oxidize H_2O to generate hydroxyl radicals (·OH). After entering the dark phase, the afterglow emission of SMSO (centered at 470 nm) can continuously excite ZIS, enabling the release of stored electrons and sustaining radical generation. Electron spin resonance (ESR) tests confirmed the presence of ·OH signals even under dark conditions. The generated ·OH and $\cdot O_2^-$ radicals work synergistically to disrupt bacterial cell membranes, leading to leakage of cellular contents and damage to DNA and proteins. Experimental results indicated that after 1 h of illumination, the ZIS/SMSO (1∶0.5) composite achieved a sterilization rate of 28.9%, which was 2.9 times and 2.5 times higher than that of pure ZIS and pure SMSO, respectively. Importantly, the composite maintained antibacterial activity for up to 6 h in the dark after illumination ceased, with the sterilization rate increasing to 64.4%. This performance was 2.8 times and 1.9 times higher than that of ZIS (22.8%) and SMSO (33.6%) under the same dark conditions, respectively. This composite catalyst provides a new strategy for controlling biofouling in aquatic environments. However, its resistance to interference from various organic and inorganic ions in complex real water matrices, as well as its long-term stability under continuous immersion, remain critical questions that must be addressed before engineering application can be realized.

6 Conclusion and outlook

Long persistent luminescent materials (LPLs) demonstrate considerable potential in the fields of photocatalysis and electrocatalysis, offering an innovative technological pathway to address two global challenges: sustainable energy supply and environmental pollution control. Their unique "store-and-release" light capability enables them to function as an embedded light source, effectively extending the operational performance of photocatalysts and photovoltaic devices under low-light or dark conditions. In photovoltaic applications, LPLs can serve as spectral converters and light-harvesting layers to enhance solar light utilization and boosting energy conversion efficiency under illumination. In the field of catalysis, by forming heterojunctions with semiconductors, LPLs facilitate the separation of photogenerated charge carriers, suppress electron-hole recombination, strengthen redox capability, and ultimately enhance photocatalytic activity. Moreover, the "intermittent illumination" strategy based on LPLs has shown notable energy-saving potential in several studies, further highlighting the practical value of LPLs in sustainable energy and environmental remediation.

Long persistent luminescent materials (LPLs) applied in photo-/electrocatalysis can be broadly classified into two categories based on their composition: composite LPLs, which are constructed by integrating LPLs with conventional semiconductor catalysts, and single-phase LPLs (single-phase systems) that inherently possess dual "catalytic-energy storage" functions. In composite systems, the LPL component typically serves as an "embedded light source," leveraging its photon storage capability to provide sustained excitation for the semiconductor catalyst (e.g., TiO_2, g-C_3N_4) under dark or low-light conditions, thereby enabling round-the-clock catalytic activity. The design of such composites follows the principle of spectral matching, requiring effective overlap between the emission spectrum of the LPL and the absorption spectrum of the semiconductor to facilitate resonance energy transfer. The core advantage of this system lies in its functional modularity and design flexibility, as it can incorporate well-established semiconductor materials to extend their applications across diverse fields, including photocatalytic degradation, water splitting for hydrogen production, CO_2 reduction, sterilization, and photovoltaic cells. Composite systems are mainly constructed *via* two approaches: physical and chemical methods. Physical methods, such as mechanical mixing, grinding, or coating, achieve component bonding through weak interactions like van der Waals forces or mild mechanical interlocking. These techniques are straightforward and help preserve the intrinsic properties of each component. Early studies on composite long-afterglow photocatalysts and certain long-afterglow devices predominantly followed this pathway. However, the resulting interfacial contact tends to be loose, leading to limited charge transfer efficiency. Performance improvements in such systems rely mainly on

photoluminescence-based resonance energy transfer, resulting in only moderate synergistic effects. Chemical methods achieve stronger coupling by constructing heterojunctions through approaches such as *in situ* growth, solvothermal synthesis, or chemical bonding. These methods enable the formation of chemical bonds or strong electrostatic interactions at the interface, resulting in tight contact between the components. This not only significantly enhances interfacial charge transfer but also allows band engineering to achieve spatial separation of charge carriers, thereby improving the redox capability and catalytic performance of the photocatalyst under illumination. Nevertheless, this method involves more complex synthesis conditions, may affect the intrinsic photon-storage properties of the LPL component, and demands higher demands on interfacial engineering design. In summary, chemical methods are generally more suitable for deep catalytic reactions where high activity and stability are paramount, whereas physical methods may be advantageous in applications where preserving the intrinsic light-storage properties of the LPLs is a priority, or where avoiding complex interfacial effects is desirable, such as in certain designs of photovoltaic cells.

Unlike composite systems that rely on relatively mature semiconductor catalysts, single-phase long persistent luminescent materials (LPLs) aim to achieve intrinsic multifunctional integration within the material itself—combining efficient light storage, delayed emission, and catalytic activity. Research on photocatalysis/electrocatalysis in this system remains in its preliminary exploration and development phase. Current studies primarily employ strategies such as ion doping (e.g., introducing shallow traps *via* Ga^{+}), defect engineering (e.g., oxygen vacancy modulation), or surface modification (e.g., loading Ag nanoparticles) to optimize the carrier storage capacity, release kinetics, and surface reactivity of the materials. Their key advantage lies in their structural homogeneity, which fundamentally avoids charge-transfer losses and stability issues associated with heterogeneous interfaces. However, this approach also imposes higher demands on the material's band structure, defect chemistry, and active-site design, while the coordination of multiple functions and balancing of performance remain significant challenges. Furthermore, the expansion of applicable systems based on this strategy is still relatively limited.

Despite notable progress in long-persistent photo-/electrocatalysis, several critical challenges persist, and future efforts should focus on the following directions: First, in terms of material design, current research—whether on composite or single-phase systems—is heavily concentrated on aluminate- and silicate-based LPLs, mainly because the balance between trap energy levels and thermal disturbance in these systems has been well studied, facilitating room-temperature long afterglow. However, constrained by the scarcity and high cost of rare-earth elements (e.g., Dy^{+}), there is an urgent need to explore new host materials that are non-rare-earth or low in rare-earth content. This includes developing new, inexpensive, and environmentally friendly material systems activated by transition metal ions (e.g., Cr^{+}, Mn^{+}) or main-group elements (e.g., Bi^{+}), as well as organic-inorganic hybrid materials.

Second, at the level of mechanism research, a mature characterization pathway has been established to elucidate the "excitation-trapping-release" mechanism of LPLs. Specifically, these include: using basic spectroscopy to identify luminescent centers and phenomena; determining the host structure *via* structural characterization; analyzing key defects with techniques such as electron spin resonance (ESR), photoconductivity (PC), and positron annihilation lifetime spectroscopy (PALS); quantifying trap depth and distribution through thermoluminescence (TL); and correlating microscopic defects with macroscopic performance *via* X-ray absorption spectroscopy (XAS) and synchrotron-based methods (e.g., SR-XAS) at atomic and electronic band-structure levels. Nevertheless, most current studies remain at the stage of mechanistic description and have yet to establish quantitative structure-activity relationships between material structures and macroscopic performance. To overcome this limitation, future work could employ dynamic characterization techniques such as transient absorption and *in situ* spectroscopy to capture real-time reaction information. Additionally, integrating first-principles calculations and machine-learning methods could systematically investigate how various defects regulate key parameters (e.g., trap energy levels, carrier effective mass, surface adsorption energy), ultimately building predictive "structure-performance" models to guide the targeted design and optimization of materials.

Third, existing studies still lack data on catalytic stability under complex environmental conditions, such as high salinity, wide pH ranges, coexisting pollutants, complex ionic backgrounds, and natural day-night light cycles. Therefore, subsequent research should establish corresponding experimental protocols and data-reporting standards to ensure comparability and continuity, providing a reliable reference for future studies. Simultaneously, the feasibility of large-scale material production remains a critical issue requiring breakthroughs. To truly advance catalytic materials toward practical application, it is essential to overcome the challenges of developing scalable and controllable synthesis processes.

Finally, future research on LPL-based photo-/electrocatalysis should pursue interdisciplinary expansion into new directions. Current studies mainly focus on photocatalytic organic degradation, water splitting for hydrogen evolution, and photovoltaic cells. Should further efforts be extended to explore LPL applications in frontier areas such as the highly selective reduction of CO_2 to high-value chemicals, nitrogen fixation for ammonia synthesis, reduction and immobilization of heavy-metal ions, and integrated energy conversion with chemical synthesis. Furthermore, the response behavior of LPLs under coupled physical fields (thermal, electrical, magnetic, etc.) should be investigated to

develop smart responsive catalytic systems enabling on-demand activation/deactivation and precise regulation of catalytic processes. In summary, long-persistent photo-/electrocatalysis is a vibrant and interdisciplinary frontier. Future research will require collaboration across materials science, chemistry, photonics, and engineering to drive this green technology toward substantive contributions in addressing energy and environmental challenges.

Declaration of Competing Interest

The authors declare no conflict of interest.

References

[1] QIAO J, ZHOU G, ZHOU Y, et al. Divalent europium-doped near-infrared-emitting phosphor for light-emitting diodes[J]. Nat Commun, 2019, 10(1): 5267.

[2] ZHANG T, ZHOU J, LI H, et al. Stable lignin-based afterglow materials with ultralong phosphorescence lifetimes in solid-state and aqueous solution[J]. Green Chem, 2023, 25(4): 1406−1416.

[3] VAIDYANATHAN S. Recent progress on lanthanide-based long persistent phosphors: An overview[J]. J Mater Chem C, 2023, 11(26): 8649−8687.

[4] WANG P, ZHENG D, LIU S, et al. Producing long afterglow by cellulose confinement effect: A wood-inspired design for sustainable phosphorescent material[J]. Carbon, 2021, 171: 946−952.

[5] XU J, TANANE S. Persistent luminescence instead of phosphorescence: History, mechanism, and perspective[J]. J Lumin, 2019, 205: 581−620.

[6] KABE R, ADACHI C. Organic long persistent luminescence[J]. Nature, 2017, 550(7676): 384−387.

[7] LI D, WANG Y, XU K, et al. Persistent luminescent and photocatalytic properties of $Zn_xGa_2O_{3+x}$ ($0.8 \leqslant x \leqslant 1$) phosphors[J]. RSC Adv, 2015, 5(27): 20972−20975.

[8] GUO Y, WANG Q, LIU S, et al. A brief review: the application of long afterglow luminescent materials in environmental remediation[J]. RSC Adv, 2023, 13(2): 16145−16153.

[9] SINGH V, CHAKRADHAR R P S, RAO J L, et al. Photoluminescence and EPR studies of Cr-doped hibonite ($CaAl_{12}O_{19}$) phosphors[J]. Solid State Sci, 2008, 10(11): 1525−1532.

[10] MATSUZAWA T, AOKI Y, TAKEUCHI N, et al. A new long phosphorescent phosphor with high brightness, $SrAl_2O_4$: Eu^{2+}, Dy^{3+}[J]. J Electrochem Soc, 1996, 143(8): 2670.

[11] ESTEFANIA ROJAS-HERNANDEZ R, RUBIO-MARCOS F, ANGEL RODRIGUEZ M, et al. Long lasting phosphors: $SrAl_2O_4$: Eu, Dy as the most studied material[J]. Renewable Sustainable Energy Rev, 2018, 81: 2759−2770.

[12] LIANG L, CHEN J, SHAO K, et al. Controlling persistent luminescence in nanocrystalline phosphors[J]. Nat Mater, 2023, 22(3): 289−304.

[13] LIU Y, WANG Z, MIAO K, et al. Research progress on near-infrared long persistent phosphor materials in biomedical applications[J]. Nanoscale Adv, 2022, 4(23): 4972−4996.

[14] YU J, LUO M, LV Z, et al. Recent advances in optical and optoelectronic data storage based on luminescent nanomaterials[J]. Nanoscale, 2020, 12(46): 23391−23423.

[15] WANG X, LI C. Roles of phase junction in photocatalysis and photoelectrocatalysis[J]. J Phys Chem C, 2018, 122(37): 21083−21096.

[16] KANG F, SUN G, BOUTINAUD P, et al. Recent advances and prospects of persistent luminescent materials as inner secondary self-luminous light source for photocatalytic applications[J]. Chem Eng J, 2021, 403: 126099.

[17] CHEN X, SHEN S, GUO L, et al. Semiconductor-Based Photocatalytic Hydrogen Generation[J]. Chem Rev, 2010, 110(11): 6503−6570.

[18] PEI L, MA Z, ZHONG J, et al. Oxygen vacancy-rich $Sr_2MgSi_2O_7$: Eu^{2+}, Dy^{3+} long afterglow phosphor as a round-the-clock catalyst for selective reduction of CO_2 to CO[J]. Adv Funct Mater, 2022, 32(49): 2208565.

[19] LI Y, GECEVICIUS M, QIU J. Long persistent phosphors-from fundamentals to applications[J]. Chem Soc Rev, 2016, 45(8): 2090−2136.

[20] SHARMA T, NGUYEN T T H, NGUYEN N H, et al. Computational, optical and feasibility studies of organic luminescence TMB-PPT blend for photovoltaic application[J]. Heliyon, 2024, 10(4): e26048.

[21] LI H, YIN S, WANG Y, et al. Persistent fluorescence-assisted $TiO_{2-x}N_y$-based photocatalyst for gaseous acetaldehyde degradation[J]. Environ Sci Technol, 2012, 46(14): 7741−7745.

[22] LIZ, LIU H, ZHANG X B. Reactive oxygen species-mediated organic long-persistent luminophores light up biomedicine: From two-component separated nano-systems to integrated uni-luminophores[J]. Chem Soc Rev, 2024, 53(22): 11207−11227.

[23] CHEN X Y, MA C, LI X X, et al. Novel necklace-like $MA_{l2}O_4$: Eu^{2+}, Dy^{3+} (M = Sr, Ba, Ca) phosphors via a CTAB-assisted solution-phase synthesis and postannealing approach[J]. J Phys Chem C, 2009, 113(7): 2685−2689.

[24] SU G, SHEN R, TAN J, et al. Progress on the application of long persistent phosphors in photocatalytic system[J]. Chem J Chin Univ, 2020, 41(11): 2404−2414.

[25] BIDWAI D, SAHU N K, DHOBLE S J, et al. Review on long afterglow nanophosphors, their mechanism and its application in round-the-clock working photocatalysis[J]. Method Appl Fluores, 2022, 10(3): 032001.

[26] NIDHANKAR A D, GOUDAPPAGOUDA, WAKCHAURE V C, et al. Efficient metal-free organic room temperature phosphors[J]. Chem Sci, 2021, 12(12): 4216−4236.

[27] LIN C, WU Z, MA H, et al. Charge trapping for controllable persistent luminescence in organics[J]. Nat Photonics, 2024, 18(4): 350−356.

[28] SAKAR M, CHINH-CHIEN N, MANH-HIEP V, et al. Materials and mechanisms of photo-assisted chemical reactions under light and dark conditions: Can day-night photocatalysis Be achieved?[J]. ChemSusChem, 2018, 11(5): 809−820.

[29] YANG X, WATERHOUSE G I N, LU S, et al. Recent advances in the design of afterglow materials: Mechanisms, structural regulation strategies and applications[J]. Chem Soc Rev, 2023, 52(22): 8005−8058.

[30] DING Y, YE Y, WANG C, et al. "Light battery" role of long afterglow phosphor for round-the-clock environmental photocatalysis[J]. J Cleaner Prod, 2024, 450: 142041.

[31] KATTEL G R. State of future water regimes in the world's river basins: Balancing the water between society and nature[J]. Crit Rev Environ Sci Technol, 2019, 49(12): 1107−1133.

[32] LU T, WANG L, HE Y, et al. Loess surface grafted functional copolymer for removing basic fuchsin[J]. RSC Adv, 2017, 7(30): 18379−18383.

[33] PU H, TANG P, ZHAO L, et al. Preparation of a carboxymethyl β-cyclodextrin polymer and its rapid adsorption performance for basic fuchsin[J]. RSC Adv, 2020, 10(35): 20905−20914.

[34] MAKOFANE A, MOTAUNG D E, HINTSHO-MBITA N C. Photocatalytic degradation of methylene blue and sulfisoxazole from water using biosynthesized zinc ferrite nanoparticles[J]. Ceram Int, 2021, 47(16): 22615−22626.

[35] CIONTI C, PARGOLETTI E, FALLETTA E, et al. Combining pH-triggered adsorption and photocatalysis for the remediation of complex water matrices[J]. J Environ Chem Eng, 2022, 10(5): 108468.

[36] HORIKOSHI S, SERPONE N. Can the photocatalyst TiO_2 be incorporated into a wastewater treatment method? Background and prospects[J]. Catal Today, 2020, 340: 334−346.

[37] LIU C, LIU F, HUANG F, et al. Preparation and photocatalytic properties of alga-based CDs-Cu-TiO_2 composite material[J]. J Inorg Mater, 2021, 36(11): 1154−1162.

[38] YOON S, BIERWAGEN J, TROTTMANN M, et al. The influence of boric acid on improved persistent luminescence and thermal oxidation resistance of $SrAl_2O_4$: Eu^{2+}[J]. J Lumin, 2015, 167: 126−131.

[39] ZHANG J, PAN F, HAO W, et al. Light-storing photocatalyst[J]. Appl Phys Lett, 2004, 85(23): 5778−5780.

[40] LI H, YIN S, SATO T. Persistent deNO_x ability of $CaAl_2O_4$: (Eu, Nd)/$TiO_{2-x}N_y$ luminescent photocatalyst[J]. Nanoscale Res Lett, 2010, 6(1): 5.

[41] SHANG Y, CUI Y, SHI R, et al. Depositing Ag_3PO_4 on WO_3 hollow microspheres at room temperature for rapid photocatalytic degradation of Rhodamine B[J]. Prog Nat Sci: Mater Int, 2022, 32(3): 282−288.

[42] ZHANG M, LI F, JIANG S, et al. $CaAl_2O_4$: Eu^{2+}, Nd^{3+} anti-corrosive coating and its afterglow-catalytic process[J]. Opt Mater, 2021, 116: 111049.

[43] HAVASI V, VDRDI B, KUKOVECZ. Photocatalytic performance of $Sr_4Al_{14}O_{25}$:Eu, Dy phosphor assisted ZnO: Co+Ag nanocomposite under continuous and pulsed illumination[J]. Catal Today, 2017, 284: 107−113.

[44] LU Y, ZHANG X, CHU Y, et al. Cu_2O nanocrystals/TiO_2 microspheres film on a rotating disk containing long-afterglow phosphor for enhanced round-the-clock photocatalysis[J]. Appl Catal B: Environ, 2018, 224: 239−248.

[45] ALIABADI H M, ZARGOOSH K, AFSHARI M, et al. Synthesis of a luminescent g-C_3N_4–WO_3–Bi_2WO_6/$SrAl_2O_4$:Eu^{2+}, Dy^{3+} nanocomposite as a double z-scheme sunlight activable photocatalyst[J]. New J Chem, 2021, 45(10): 4843−4853.

[46] LI S , LIU M, WEN L, et al. Exploration of long afterglow luminescent materials composited with graphitized carbon nitride for photocatalytic degradation of basic fuchsin[J]. Environ Sci Pollut Res, 2023, 30(1): 322−336.

[47] CHEN M, LI S, WEN L, et al. Exploration of double Z-type ternary composite long-afterglow/graphitic carbon nitride@metal–organic framework for photocatalytic degradation of methylene blue[J]. J Colloid Interface Sci, 2023, 629: 409−421.

[48] BU X, LIU Y GAI, XIE C, et al. Photocatalytic composite $Sr_2MgSi_2O_7$: (Eu, Dy)/g-C_3N_4: A Z-scheme heterojunction material formed by long-afterglow phosphors and photocatalysts on round-the-clock photocatalytic degradation of methylene blue[J]. ACS Appl Opt Mater, 2023, 1(3): 688−700.

[49] WU H, WANG Z M, KOIKE K, et al. Hybridization of silver orthophosphate with a melilite-type phosphor for enhanced energy-harvesting photocatalysis[J]. Catal Sci Technol, 2017, 7(17): 3736−3746.

[50] Ma X, He S, Zhang Z, et al. Fabrication of double S-scheme $Sr_2MgSi_2O_7$: Eu^{2+}, Dy^{3+}/$ZnIn_2S_4$/UiO-66-NH_2 heterojunctions with photon storage effect for enhanced round-the-clock photocatalysis[J]. J Alloys Compd, 2025, 1010: 176993.

[51] VAIANO V, SACCO O, SANNINO D. Electric energy saving in photocatalytic removal of crystal violet dye through the simultaneous use of long-persistent blue phosphors, nitrogen-doped TiO_2 and UV-light emitting diodes[J]. J Clean Prod, 2019, 210: 1015−1021.

[52] HE F, ABULIMITI A, LI B, et al. Persistent luminescent nanoparticle-coated metal–organic frameworks for round-the-clock photocatalytic degradation of pollutants[J]. ACS Appl Nano Mater, 2023, 6(14): 12871−12881.

[53] ZHOU J, HUANG J, XIA Y, et al. Two-in-one ultraviolet persistent luminescent catalyst suitable for high concentration photodegradation[J]. Sci Total Environ, 2020, 699: 134342.

[54] HAI O, PEI M, YANG E, et al. Exploration of long afterglow luminescence materials work as round-the-clock photocatalysts[J]. J Alloys Compd, 2021, 866: 158752.

[55] ZHAO Y, DING C, ZHU J, et al. A hydrogen farm strategy for scalable solar hydrogen production with particulate photocatalysts[J]. Angew Chem Int Ed, 2020, 59(24):

9653−9658.

[56] WANG X, CHENG T, HONG H, et al. Challenges and opportunities in hydrogen storage and transportation: A comprehensive review[J]. Renew Sust Energ Rev, 2025, 219(13): 115881.

[57] WAN C, ZHOU L, SUN L, et al. Boosting visible-light-driven hydrogen evolution from formic acid over AgPd/2D g-C_3N_4 nanosheets Mott-Schottky photocatalyst[J]. Chem Eng J, 2020, 396: 125229.

[58] ZHAO W, LI Y, ZHAO P, et al. Novel Z-scheme Ag-C_3N_4/SnS_2 plasmonic heterojunction photocatalyst for degradation of tetracycline and H_2 production[J]. Chem Eng J, 2021, 405: 126555.

[59] LIU X, CHEN X, LI Y, et al. A g-C_3N_4@Au@$SrAl_2O_4$: Eu^{2+}, Dy^{3+} composite as an efficient plasmonic photocatalyst for round-the-clock environmental purification and hydrogen evolution[J]. J Mater Chem A, 2019, 7(32): 19173−19186.

[60] TU Y, CHI S, DANG J, et al. Round-the-clock efficient degradation and simultaneous hydrogen evolution over long afterglow light driven Z-scheme Cu| CuO/$SrAl_2O_4$: Eu^{2+}, Dy^{3+} photocatalyst composite film[J]. Mater Sci Semicond Process, 2024, 184: 108856.

[61] TANG J, LIU X, LIU Y, et al. Novel Z-scheme $Sr_2MgSi_2O_7$: Eu^{2+}, Dy^{3+}/Ag_3PO_4 photocatalyst for round-the-clock efficient degradation of organic pollutants and hydrogen production[J]. Chem Eng J, 2022, 435: 134773.

[62] TANG J, LIU Y, ZHANG X, et al. Fabrication of loaded Ag sensitized round-the-clock highly active Z-scheme $BiFeO_3$/Ag/$Sr_2MgSi_2O_7$: Eu^{2+}, Dy^{3+}/Ag photocatalyst for metronidazole degradation and hydrogen production[J]. J Power Sources, 2023, 580: 233433.

[63] WANG J, PAN R, YUAN Z, et al. Functionalized $Sr_2MgSi_2O_7$: (Eu, Dy)@CdS heterojunction photocatalyst for round-the-clock hydrogen production[J]. Chem Eng J, 2024, 481: 148296.

[64] ABULIMITI A, YAN P, NIU M, et al. PLNPs/SCN heterojunction composites with a green afterglow for photocatalytic hydrogen production[J]. New J Chem, 2024, 48(22): 10304−10313.

[65] LI B, ABULINITI A, TUERDI A, et al. Heterojunction composites of covalent organic frameworks grown on the surface of persistent luminescent nanoparticles for photocatalytic hydrogen evolution and degradation of organic pollutants[J]. Colloid Surface A, 2024, 700: 134792.

[66] CUI G, YANG X, ZHANG Y, et al. Round-the-clock photocatalytic hydrogen production with high efficiency by a long-afterglow material[J]. Angew Chem Int Ed, 2019, 58(5): 1340−1344.

[67] ZHAO J, SUN X, WANG Z. Ce^{3+}/Eu^{2+} doped $SrSc_2O_4$ phosphors: Synthesis, luminescence and energy transfer from Ce^{3+} to Eu^{2+}[J]. Chem Phys Lett, 2018, 691(1): 68−72.

[68] FAN Y, LIU Y, ZHANG Y, et al. Photocatalytic hydrogen and oxygen evolution performed by a long-afterglow material[J]. Inorg Chem, 2024, 63(22): 10397–10402.

[69] PARIDA B, INIYAN S, GOIC R. A review of solar photovoltaic technologies[J]. Renewable Sustainable Energy Rev, 2011, 15(3): 1625−1636.

[70] XU X, LI S, ZHANG H, et al. A power pack based on organometallic perovskite solar cell and supercapacitor[J]. ACS Nano, 2015, 9(2): 1782−1787.

[71] SUN H, PAN L, PIAO X, et al. Long afterglow $SrAl_2O_4$: Eu, Dy phosphors for CdS quantum dot-sensitized solar cells with enhanced photovoltaic performance[J]. J Mater Chem A, 2013, 1(21): 6388−6392.

[72] SUN H, PAN L, PIAO X, et al. Enhanced performance of cadmium selenide quantum dot-sensitized solar cells by incorporating long afterglow europium, dysprosium co-doped strontium aluminate phosphors[J]. J Colloid Interface Sci, 2014, 416: 81−85.

[73] DENG Y, LU S, XU Z, et al. Enhanced performance of CdS/CdSe quantum dot-sensitized solar cells by long-persistence phosphors structural layer[J]. Sci China Mater, 2020, 63(4): 516−523.

[74] TANG Q, ZHU W, HE B, et al. Rapid conversion from carbohydrates to large-scale carbon quantum dots for all-weather solar cells[J]. ACS Nano, 2017, 11(2): 1540−1547.

[75] HU Y, ZHANG X, LIU Y, et al. Study of NIR long afterglow luminescent materials are used in silicon solar cells to produce electricity under dark condition[J]. Opt Mater, 2024, 150: 115217.

[76] ZHANG H, SUN M, ZHANG J, et al. High performance long-afterglow phosphor-based $ZnIn_2S_4$/$Sr_2MgSi_2O_7$: Eu^{2+}, Dy^{3+} photocatalyst capable of dark state long-term application for photocatalytic sterilization[J]. J Alloys Compd, 2025, 1010: 176711.

清洁能源与环境保护: 长余辉材料在光/电催化领域的应用

黄海燕[1]，杨亚荣[1]，赵卓雅[1]，刘丁艺[1]，王　璇[1]，吴淑琪[1,*]，覃　勇[2,*]，苗娇娇[1,*]

（1. 西北工业大学生命科学学院 生物与催化交叉研究中心, 陕西 西安 710072;

2. 青岛科技大学 材料科学与工程学院, 山东 青岛 266042）

摘　要: 长余辉发光材料 (LPLs) 凭借其独特的光生载流子存储与可控释放能力, 在光/电催化领域展现出了巨大潜力, 为环境治理与可持续能源技术提供了创新解决方案。本工作主要综述了 LPLs 在光/电催化中的研究进展, 概述了 LPLs 的发展历程与作用机制, 重点论述了 LPLs 在有机污染物降解、光催化制氢以及光伏电池等方向的应用, 并总结归纳了该材料的设计策略和研究体系。还探讨了 LPLs 目前研究存在的局限与挑战, 展望了其未来研究方向, 以助 LPLs 从基础研究向实际能源与环境应用的转化。

关键词: 催化; 长余辉; 降解; 氢气; 太阳能

中图分类号: O643　　**文献标识码:** A

作者简介:



黄海燕, 硕士研究生。目前主要从事电催化领域的研究工作, 123456789000@mail.nwpu.edu.cn。



吴淑琪, 博士, 副教授, 主要从事长余辉光学分子影像和疾病诊疗的研究, sqwu@nwpu.edu.cn。



杨亚荣, 博士研究生。主要从事电化学传感方面的研究, yyr@mail.nwpu.edu.cn。